Review

State-of-the-Art Review of Artificial Intelligence in Environmental Geophysics and Geotechnical Engineering

Adedibu Sunny Akingboye * , Andy Anderson Bery , Mbuotidem David Dick , Babangida Mohammed Ahmed , Temitayo Olamide Ale , Adeyemi Oludapo Olusola

Posted Date: 22 May 2026

doi: 10.20944/preprints202605.1511.v1

Keywords: artificial intelligence; machine/deep learning; physics-informed learning; multimodal data fusion; engineering geophysics; geotechnical engineering

 doi:10.20944/preprints202605.1511.v1

Review

State-of-the-Art Review of Artificial Intelligence in Environmental Geophysics and Geotechnical Engineering

Adedibu Sunny Akingboye [1,2,3,4,*], Andy Anderson Bery [1,2], Mbuotidem David Dick [1,2,5], Babangida Mohammed Ahmed [1,2,6], Temitayo Olamide Ale [3] and Adeyemi Oludapo Olusola [4]

[1] Geophysics Programme, School of Physics, Universiti Sains Malaysia, 11800 USM, Penang, Malaysia
[2] Earth System Processes and Hazard Modeling Center, Geophysics Programme, School of Physics, Universiti Sains Malaysia, 11800 USM, Penang, Malaysia
[3] Department of Earth Sciences, Adekunle Ajasin University, 001 Akungba-Akoko, Ondo State, Nigeria
[4] Faculty of Environmental and Urban Change, York University, 4700 Keele Street, Toronto, ON, M3J 1P3, Canada
[5] Department of Science Technology, Akwa Ibom State Polytechnic, Ikot Osurua, Ikot Ekpene, Akwa Ibom State, Nigeria
[6] Department of Applied Physics, Federal University of Technology, Babura, Jigawa State, Nigeria
* Correspondence: asakingboye@usm.my or adedibu.akingboye@aaua.edu.ng

Highlights

- A unified AI–EGGE framework integrating geophysics, environmental systems, geotechnics, and AI
- Integrate ML, DL, physics-informed learning, multimodal fusion, and trustworthy AI in one framework
- Enables joint geophysical–environmental–geotechnical modeling for high-resolution subsurface intelligence
- Identifies key limits: data heterogeneity, ill-posed inversion, generalization gaps, validation issues
- Defines roadmap for physics-integrated AI, digital twins, adaptive sensing, and real-world deployment

Abstract

Artificial intelligence (AI) is transforming environmental geophysics and geotechnical engineering (EGGE), shifting practice from empirical and deterministic workflows toward data-rich, physics-consistent, and decision-oriented subsurface intelligence. This review synthesizes advances in machine learning, deep learning, physics-informed and theory-guided modeling, multimodal data fusion, uncertainty-aware and explainable AI, and intelligent sensing for near-surface, environmental, and geotechnical systems. It presents an integrated framework linking physics-informed AI, multimodal fusion, and regulatory pathways for deployment in EGGE, bridging methodological innovation and operational adoption. These advances enable high-resolution subsurface characterization, lithological and geotechnical profiling, hydro-geomechanical parameter estimation, groundwater assessment, geohazard forecasting, and infrastructure monitoring, marking a transition to field-validated decision-support systems for early warning, risk-informed design, and climate-resilient management. Key challenges include data heterogeneity, cross-scale inconsistency, limited ground truth, fusion complexity, ill-posed inversion, weak generalization across geological and climatic regimes, and insufficient interpretability, uncertainty quantification, and validation for engineering decisions. Regulatory gaps further constrain adoption. A roadmap emphasizes scalable physics-integrated AI, next-generation multimodal fusion, interpretable and uncertainty-aware modeling, edge-cloud digital twins, adaptive data acquisition, and standardized benchmarking. AI

 doi:10.20944/preprints202605.1511.v1

can redefine EGGE through resilient, sustainability-aligned subsurface intelligence if scientific rigor and governance advance in parallel.

Keywords: artificial intelligence; machine/deep learning; physics-informed learning; multimodal data fusion; engineering geophysics; geotechnical engineering

1. Introduction

Artificial intelligence (AI) is reshaping environmental geophysics and geotechnical engineering (EGGE) through the AI–EGGE paradigm, redefining how near-surface systems are characterized, modeled, and managed under increasing environmental and infrastructure pressures [1–4]. While conventional and physics-based approaches remain foundational, they often struggle to represent the nonlinear behavior, uncertainty, and multiscale heterogeneity that govern surface–subsurface processes [5–7]. The rapid growth of geophysical, geotechnical, and environmental datasets has positioned AI as a powerful complement, enabling the extraction of complex patterns from high-dimensional data and improving inference where traditional inversion and regression are poorly constrained [8,9]. By learning relationships among geophysical observables, mechanical properties, and environmental indicators, AI enhances prediction, interpretability, and decision support in subsurface characterization [10–12].

The adoption of AI in Earth sciences has progressed from early expert systems and regression-based models to modern machine learning (ML), including unsupervised clustering algorithms such as k-means, fuzzy c-means, and self-organizing maps, capable of extracting spatial, temporal, and structural features from complex datasets [13–16]. These foundations have further advanced into deep learning (DL) architectures, e.g., feedforward, convolutional, recurrent, autoencoder, generative, and graph-based networks, that autonomously learn hierarchical representations from high-dimensional data [17–20]. More recently, hybrid and physics-informed approaches have emerged, explicitly embedding governing physical constraints within data-driven learning to support multi-physics integration across geophysical and geotechnical domains [21–23]. These developments now enable coupled modeling of electrical (resistivity, induced polarization [IP], self-potential [SP]), electromagnetic (EM), seismic (refraction tomography and multichannel analysis of surface waves [SRT, MASW], reflection), ground-penetrating radar (GPR), magnetic, gravity, radiometric, and borehole datasets within unified AI-driven predictive frameworks.

EGGE are inherently complementary disciplines focused on imaging, characterizing, and engineering the near-surface critical zone, where hydrological, geological, geochemical, and geomechanical processes interact [24,25]. Environmental geophysics provides noninvasive, continuous subsurface imaging through the aforementioned geophysical datasets, enabling delineation of subsurface structure, fractures, contaminant pathways, voids, cavities, hydrogeological boundaries, etc [26–28]. Geotechnical engineering complements these observations through direct characterization of soil and rock behavior using the standard penetration test (SPT/SPT-N), cone penetration test (CPT/CPT-qc), rock quality designation (RQD), rock mass quality (RMQ), and related indices [29,30]. Integrating these heterogeneous datasets within AI-enabled workflows, hereafter termed AI–EGGE, unites continuous subsurface imaging with discrete mechanical and material properties, enabling physics-consistent feature extraction, improved prediction of geotechnical indices from geophysical attributes, and enhanced spatial resolution of geomechanical parameters.

Applications of AI–EGGE are expanding rapidly across surface–subsurface and infrastructure systems. Supervised and ensemble models have been used to predict shear-wave velocity (Vs) and stiffness from ERT, MASW, or SRT [6,21,31], and infer P-wave velocity (Vp), dynamic moduli, and soil or rock integrity using ERT–SRT or ERT–IP correlations [13,27,32–34]. Unsupervised ML and DL further improve mapping of subsurface heterogeneity, facies, transition zones, and landslide precursors from integrated geophysical–borehole data [35–37]. Hybrid and physics-informed

 doi:10.20944/preprints202605.1511.v1

models, including Bayesian and metaheuristic–DL couplings, enhance estimation of integrity, deformation moduli, and stress–strain behavior for slope, tunnel, and foundation design [38,39]. Cross-disciplinary DL architectures, such as encoder–decoders, convolutional neural networks (CNNs), U-Nets, vision transformers (ViTFs), and graph neural networks (GNNs), extend AI–EGGE to multi-source spatiotemporal modeling [18,40,41]. By integrating gravity, thermal, and hydrogeological indicators, these models support improved contaminant tracking, groundwater dynamics, deformation monitoring, and resilience planning [42,43]. Collectively, they are advancing intelligent digital-twin–like systems and scenario-based simulation for infrastructure resilience and environmental risk management [3,44].

Given this background, this review consolidates recent theoretical and practical advances in AI–EGGE within a unified workflow framework (Figure 1). Specifically, the review: (i) synthesizes the historical and conceptual development of AI methodologies relevant to EGGE; (ii) examines strategies for data integration, feature engineering, and cross-domain coupling between geophysical and geotechnical datasets; (iii) reviews representative applications and case studies linking geophysical attributes with geotechnical indices; (iv) critically assesses persistent challenges related to data scarcity, generalization, interpretability, and validation; and (v) outlines pathways toward physically grounded, uncertainty-aware, and explainable AI (XAI) systems. Guided by this structure, the paper progresses from methodological foundations to integrated applications and forward-looking perspectives on environmental-engineering-grade AI for near-surface characterization.

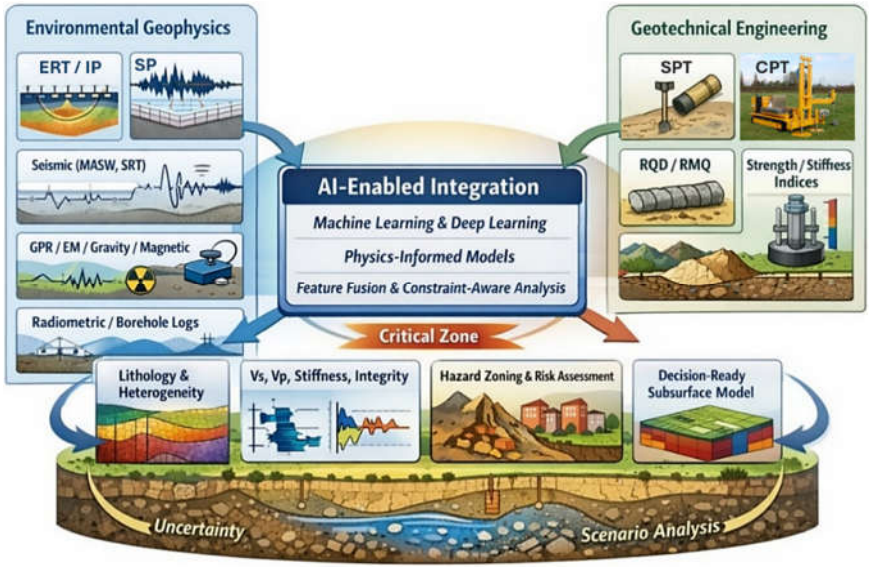

Figure 1. Systematic workflow of the AI–EGGE review framework.

2. Environmental Geophysics and Geotechnical Engineering: Foundations of AI–EGGE

The evolution of AI, from early neuron models in the 1940s through the first "golden age" of the 1950s–1960s, subsequent stagnation cycles, and the modern DL era, has progressively driven the convergence of geophysical and geotechnical domains by enabling multimodal data fusion, hierarchical feature learning, and predictive modeling across heterogeneous surface–subsurface datasets [45]. Conventional EGGE workflows, however, struggle to resolve nonlinear interactions and spatiotemporal coupling governing near-surface processes. These limitations motivate AI–EGGE as an integrative paradigm augmenting physics-based methods with data-driven learning for holistic subsurface characterization and resilience-oriented engineering. This Section outlines the core principles, data structures, and methodological foundations underpinning AI–EGGE.

 doi:10.20944/preprints202605.1511.v1

2.1. Environmental Geophysics: Methods, Capabilities, and Integrated Applications

Environmental geophysics employs noninvasive near-surface techniques to characterize subsurface conditions controlling groundwater flow, contamination, land-use planning, and ecosystem resilience [12,46]. Core methods include ERT/IP, GPR, time- and frequency-domain EM, seismic approaches (SRT, MASW), and remote sensing. ERT delineates conductivity contrasts linked to aquifers, saline intrusion, and contaminant plumes but remains sensitive to saturation, temperature, and pore-fluid chemistry [28,36,47]. IP complements ERT by capturing capacitive responses associated with clay content and mineral surface properties, enhancing lithological and contaminant discrimination [27,48]. GPR provides high-resolution imaging in resistive environments yet attenuates in conductive media [25,49], while EM offers rapid coverage at lower vertical resolution [47,50]. Seismic methods (Vs, Vp) yield elastic, stiffness, and rippability, strengthening interpretation when integrated with electrical properties [13,33]. Remote sensing supplies regional constraints on land use, vegetation stress, and recharge variability [51,52]. Multi-method integration, joint inversion, and AI-driven fusion reduce non-uniqueness, improve uncertainty quantification (UQ), and advance physics-informed multi-physics and ML/DL frameworks [4,9].

Computational advances and autonomous sensing technologies are accelerating operational deployment [53,54]. Two dominant trends emerge: (1) fusion of geophysical and Earth observation (EO) datasets using statistical, geostatistical, and ML/DL frameworks for time-lapse characterization and forecasting, and (2) adoption of UAVs, robotic platforms, and dense sensor networks delivering high-spatiotemporal data streams. Multispectral and hyperspectral imagery detect land-surface dynamics, while field geophysics constrains subsurface structure [55,56]. Multi-sensor fusion is increasingly demonstrated in practice: Gholizadeh et al. [57] merged satellite data with ERT for regional soil-contamination mapping; Omolaiye et al. [58] integrated geophysical and remote-sensing datasets with hydrogeological models to predict groundwater availability in a semi-arid Nigerian basin; and Davis et al. [51] reviewed the convergence of sensor-based monitoring, computational techniques, and Internet of Things (IoT) for soil and groundwater contamination assessment. These hybrid approaches support integrated hydro-environmental modeling and watershed-scale decision-making. Physics-informed ML, joint inversion, and cloud-based processing further reduce interpretive ambiguity, enable transfer learning under data scarcity, and support adaptive survey design. The convergence of autonomous sensing, AI-driven processing, and cloud orchestration now underpins AI–EGGE, shifting practice from method-centric surveys toward integrated subsurface intelligence [39,59].

2.2. Geotechnical Engineering: Testing, Instabilities, Monitoring, and Computational Integration

Geotechnical engineering focuses on the mechanical and hydraulic behavior of soils and rocks under natural and engineered loading. Conventional in-situ and laboratory tests—SPT, CPT, RQD/RMQ, consolidation and shear testing, seismic profiling, and electrical methods—remain central to evaluating bearing capacity, settlement, and slope stability [14,30]. While deterministic datasets historically supported empirical correlations and factor-of-safety approaches, sensitivity to heterogeneity and uncertainty has driven the adoption of probabilistic and performance-based frameworks [60,61]. Advanced seismic testing constrains dynamic properties essential for performance-based design, while reliability methods propagate parameter uncertainty through safety and serviceability assessments [62,63]. These developments reinforce the need for integrated multi-test characterization.

Advances in non-destructive testing (NDT) have expanded the geotechnical toolkit [64]. GPR, ERT, and IP enable high-resolution subsurface imaging without disturbance, enhancing data triangulation when combined with conventional tests. Probabilistic slope-stability modeling, spatial random fields, and Bayesian updating now support quantified, scenario-based risk assessment for design and mitigation [65], moving practice beyond deterministic parameters. NDT and time-lapse geophysical monitoring also capture construction effects and seasonal hydromechanical variability [26,66]. These capabilities support improved foundation design, slope-stability evaluation, and

 doi:10.20944/preprints202605.1511.v1

excavation planning [60,67]. Distributed fiber-optic sensing (DFOS), including Brillouin-based methods, optical time-domain reflectometry, distributed temperature sensing, and distributed acoustic sensing (DAS), provides dense, continuous measurements of strain, temperature, and acoustic response along structural elements and slopes [68,69]. These streams enable early detection of deformation and instability precursors, although installation, calibration, and data-management challenges persist [70]. Coupled with AI-driven anomaly detection and explainable ML, DFOS supports adaptive early-warning systems.

Climate-driven variability within the near-surface critical zone is redefining boundary conditions and increasing service-life uncertainty, necessitating coupled hydrometeorological–geotechnical models [51,71]. AI and optimization approaches increasingly support scenario-based slope-failure assessment under future climatic pathways by integrating testing, monitoring, and physical modeling, which are central to computational geotechnics [8,72]. These enable the prediction of soil classification, shear strength, liquefaction potential, bearing capacity, and rock-mass indices [6,73,74]. Ensemble learners, e.g., random forest (RF), perform robustly under noisy, heterogeneous datasets [75], while DL captures nonlinear and spatial dependencies when adequately trained [76,77]. Coupling probabilistic modeling with optimization techniques such as particle swarm optimization (PSO) and genetic algorithms (GAs) improves slope-stability analysis through enhanced parameter calibration and sensitivity assessment [78]. Statistical and data-driven analytics further improve soil behavior interpretation under varying loading and environmental conditions [6,42]. Concerns regarding generalization and interpretability are accelerating hybrid and physics-informed ML frameworks embedding constitutive constraints [11,41].

2.3. Cross-Domain Synthesis in AI–EGGE

AI–EGGE paradigms integrate environmental geophysics and geotechnical engineering within a unified intelligence-driven decision-support framework anchored on three pillars: (i) observational layers (multi-method geophysics, geotechnical testing, DFOS), (ii) computational cores (joint inversion, probabilistic inference, physics-informed/hybrid ML/DL, metaheuristic optimization), and (iii) operational outputs (forecasting, anomaly detection, early warning, decision support). Convergence emerges when geophysical, EO, and monitoring datasets are fused with well logs, CPT/SPT, and DFOS into harmonized feature spaces powering physics–ML hybrid models. These systems enhance subsurface interpolation, contaminant-pathway mapping, slope-instability forecasting, and foundation assessment under transient hydro-mechanical and climatic forcing. Three frontiers accelerate this transition: (a) multi-physics joint inversion reducing ambiguity and improving UQ relative to sequential workflows; (b) physics-informed ML embedding conservation and constitutive laws to preserve realism under sparse data; and (c) cloud–edge infrastructures enabling real-time ingestion, adaptive updating, and automated alerts. Collectively, these advances shift practice toward continuous, intelligence-driven subsurface monitoring, the hallmark of AI–EGGE.

Operationalization depends on interpretability, data integrity, and stakeholder trust. XAI and UQ remain essential where outputs inform safety-critical or regulatory decisions, such as contaminant-transport risk to water sources, foundation reliability assessments, or slope failure warnings in inhabited areas [79–81]. Current research highlights the need for transparent hybrid models (e.g., surrogate modeling with uncertainty bounds), standardized data-provenance protocols, and harmonized sensor-calibration and inversion workflows. Socio-technical factors, such as capacity building, data governance, interoperability, and regulatory alignment [82,83], will ultimately govern AI–EGGE's real-world impact. Establishing robust, traceable pipelines from sensing to decision-making is, therefore, as critical as improving predictive accuracy.

3. AI Techniques in EGGE

AI enables capture of nonlinear, heterogeneous, and spatiotemporally variable subsurface relationships that physics-only methods struggle to resolve, especially under data scarcity [10,84].

 doi:10.20944/preprints202605.1511.v1

Multimodal data fusion strengthens AI–EGGE by harmonizing information from diverse sensing and testing modalities into a unified analytical framework for subsurface characterization. Figure 2 summarizes the three main fusion strategies—early, middle, and late—and their roles in enhancing robustness, generalization, and interpretability across supervised, unsupervised, hybrid, and physics-informed ML/DL workflows. Early fusion concatenates calibrated inputs (e.g., resistivity, Vp, Vs, SPT-N, RQD) into a single feature space; middle fusion integrates learned representations; and late fusion combines modality-specific predictions via averaging, stacking, or uncertainty-weighted ensembling. Early fusion suits co-registered data, middle fusion handles heterogeneous inputs, and late fusion is preferred when modalities differ and uncertainty must be addressed. AI-driven fusion improves efficiency and sustainability by reducing investigation time and cost while enhancing spatial coverage and interpretational consistency.

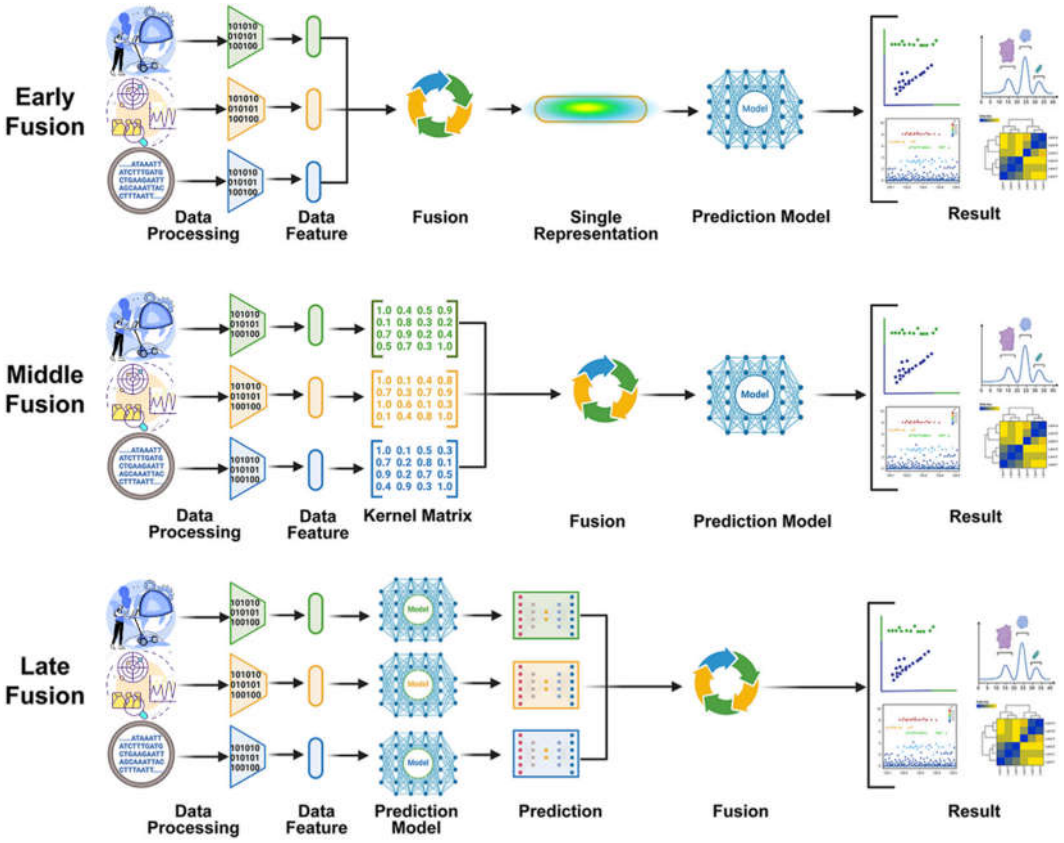

Figure 2. AI-driven data fusion strategies (modified after [45]), illustrating data-, feature-, and decision-level fusion across supervised, unsupervised, hybrid, and physics-informed AI–EGGE workflows.

Supervised, clustering, and ensemble ML methods now link geophysical attributes with mechanical, hydrogeological, and geochemical soil–rock properties, improving spatial coverage, consistency, and investigation efficiency. DL architectures, including deep neural networks (DNNs), CNNs, recurrent neural networks (RNNs), long short-term memory (LSTMs), autoencoders (AEs), transformers (TFs), generative algorithms (GAs), generative adversarial networks (GANs), and physics-informed neural networks, further extract latent features from multimodal datasets for high-resolution 2D/3D subsurface modeling, temporal analysis, anomaly detection, contaminant mapping, and deformation forecasting [10]. AI-driven analytics integrate multi-temporal satellite, geophysical, and sensor data to assess contamination, groundwater vulnerability, and soil degradation, enabling early warning and decision support [72]. Increasing engineering complexity has accelerated hybrid models that fuse geophysical insight with geotechnical parameterization. Feedforward neural networks, especially multilayer perceptrons (MLPs), remain effective for regression and classification of subsurface properties [85]. Recent advances include GAN-based synthetic data generation for

 doi:10.20944/preprints202605.1511.v1

inversion and physics-informed models that embed governing constraints to improve generalization and physical consistency [30].

3.1. Supervised and Unsupervised Learning in AI–EGGE

Supervised and unsupervised learning underpin AI–EGGE by enabling automated prediction, pattern discovery, subsurface characterization, and decision support across integrated geophysical–geotechnical investigations. They are widely applied to model and predict Vs, Vp, elastic moduli, SPT-N and CPT-qc values, compressive strength, bedrock depth, fracture density, porosity, weathering grade, and geohazard susceptibility using geophysical, remote sensing, and geospatial methods.

3.1.1. Supervised Learning

Supervised learning establishes quantitative relationships between input variables and labeled outputs, enabling the estimation of key geotechnical and subsurface integrity parameters from surface and borehole datasets [78,86,87]. Common approaches include linear, multiple, polynomial, and regularized regression methods—simple linear regression (SLR), multiple linear regression (MLR), least absolute shrinkage and selection operator (LASSO), and Ridge regression—alongside support vector machines (SVMs), k-nearest neighbors (KNN), decision trees (DT), RF, M5 model trees, extremely randomized trees (XRT), gradient boosting machines (GBMs) and variants (GBoost, XGBoost, sGBM, LightGBM), categorical boosting (CatBoost), and artificial neural networks (ANNs), including shallow and deep architectures (SNN, DNN). These models capture linear to highly nonlinear relationships and complex feature interactions, while genetic expression programming (GEP) supports interpretable symbolic regression and equation-based prediction. In general, regression-based methods model linear–polynomial trends; SVMs optimize class separation using kernel-based margins; KNN applies instance-based learning; tree-based and ensemble models enable rule-based decision modeling; boosting frameworks improve sequential ensemble performance; and SNN/DNN learn hierarchical nonlinear mappings through multi-layer feature extraction [13,31,32,42,88]. GEP is particularly beneficial in EGGE as it yields explicit analytical equations that support interpretability, parameter sensitivity assessment, and engineering adoption [24,85].

The models illustrated in Figure 3 summarize key supervised ML approaches widely used in AI–EGGE. The ANN (a) comprises an input layer, one or more hidden layers, and an output layer, where weighted connections and nonlinear activation functions learn complex input–output relationships for regression and classification in geophysical–geotechnical datasets. SVM (b) constructs an optimal separating hyperplane for classification or regression by maximizing the margin between classes, where training samples are represented as vectors $x_i$with corresponding labels y_i, and the decision function is defined as $f(x) = w^T x + b$. Kernel functions, $K(x_i, x_j)$ (e.g., linear, polynomial, RBF), map nonlinearly separable data into a higher-dimensional feature space, enabling SVM to handle complex geophysical–geotechnical patterns; support vectors—the samples closest to the margin—control the model's decision boundary. DT (c) models split data into hierarchical decision rules at internal nodes to minimize impurity or prediction error, with leaves producing final class labels or numeric outputs; DTs are intuitive, transparent, and effective for baseline geotechnical assessments. RF (d) constructs an ensemble of k decision trees using bootstrap sampling and random feature selection, with individual predictions aggregated through majority voting (classification) or averaging (regression) to reduce overfitting and improve generalization. GBM (e) builds trees sequentially, with each new tree fitting the residuals of the previous learner to minimize a chosen loss function; the final prediction is the additive combination of all weak learners $W_1 + W_2 + \cdots + W_n$, enabling strong nonlinear predictive capability. CatBoost (f) is an advanced gradient-boosting algorithm optimized for heterogeneous datasets with categorical variables, transforming categorical features using ordered target statistics to prevent leakage and overfitting, and building symmetric (oblivious) trees at each iteration to enhance training stability, speed, and generalization for diverse environmental/geotechnical predictors.

 doi:10.20944/preprints202605.1511.v1

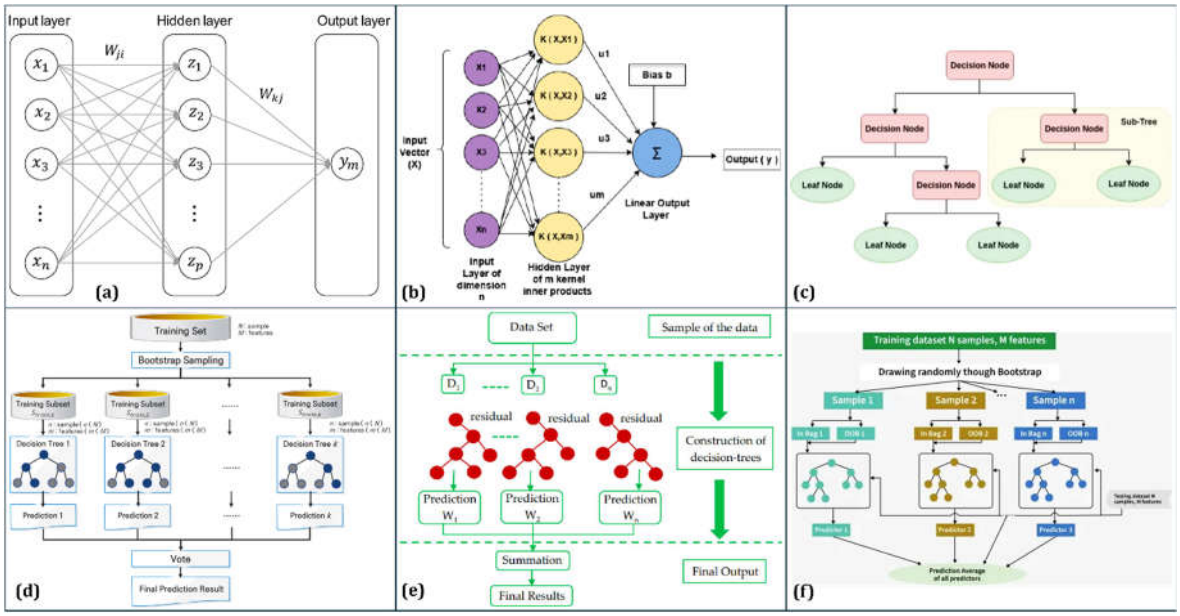

Figure 3. Schematic architectures of commonly used supervised and unsupervised ML models: (a) ANN, (b) SVM, (c) DT, (d) RF, (e) GBM, and (f) CatBoost.

Model performance is evaluated using R^2 score, mean absolute error (MAE), mean squared error (MSE), root mean squared error (RMSE), root mean squared logarithmic error (RMSLE), mean absolute percentage error (MAPE), median absolute percentage error (MdAPE), Nash–Sutcliffe Efficiency (NSE), and Willmott's Index of Agreement, with robustness assessed through repeated k-fold cross-validation, hold-out testing, residual analysis, and bias–variance diagnostics [32,75,89]. XAI techniques such as SHapley Additive exPlanations (SHAP), Local Interpretable Model-Agnostic Explanations (LIME), and Accumulated Local Effects (ALE) are increasingly used to interpret model behavior, quantify feature influence, and enhance transparency and trust in geoscience-focused machine learning applications [9].

3.1.2. Unsupervised Learning

Unsupervised learning reveals inherent structure in unlabeled datasets, enabling lithological zoning, subsurface pattern recognition, facies classification, anomaly detection, hydrogeophysical domain mapping, and structural boundary delineation without ground truth [37,90]. Unlike supervised learning, which relies on error-based metrics, unsupervised model quality is assessed using cluster validity and topology-preservation indices. Clustering is the most widely applied unsupervised approach in AI–EGGE: k-means partitions data into k clusters by minimizing within-cluster variance, while fuzzy c-means assigns membership degrees to better capture transitional boundaries in weathered, fractured, or hydrogeologically gradational zones [91]. As shown in Figure 4, k-means clustering (a) partitions a dataset into k clusters by assigning each input vector x_j to the cluster with the nearest centroid c_i based on a distance metric (commonly Euclidean), then updates centroids iteratively until convergence to reveal latent subsurface patterns [86].

On the other hand, self-organizing maps (SOMs) provide a topology-preserving projection of high-dimensional geophysical attributes onto a 2D neuron lattice, with 3D extensions for enhanced topology retention, supporting visualization of structural trends, material contrasts, and alteration zones [90]. In SOM (b), each neuron (i) has an associated weight vector ε_i. For each input vector x_j, neurons compete based on a similarity metric (typically Euclidean distance), and the closest neuron is identified as the Best Matching Unit (BMU) [92]. The BMU and its neighboring neurons are iteratively updated using a neighborhood function and learning rate to preserve topological structure. A Unified Distance Matrix (U-matrix, U) is commonly used to visualize the trained SOM, where low values indicate cluster interiors and high values highlight cluster boundaries. This enables

 doi:10.20944/preprints202605.1511.v1

SOM to effectively cluster geophysical–geotechnical signatures for lithological classification, anomaly detection, and environmental pattern recognition.

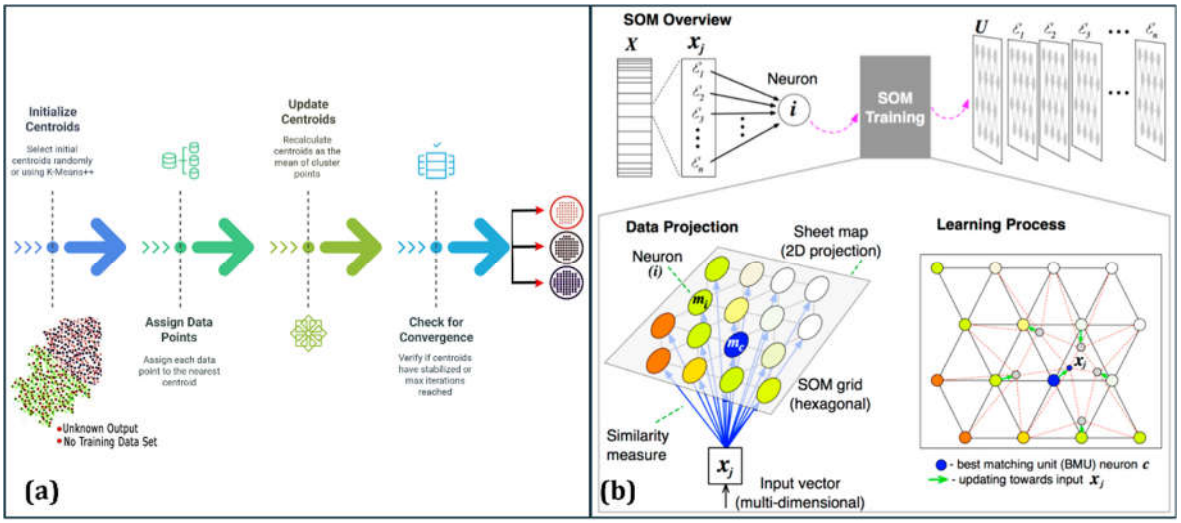

Figure 4. Schematic architectures of unsupervised ML models: (a) k-means and (b) SOM.

Advanced variants such as growing self-organizing networks (GSONs) and adaptive resonance theory networks refine cluster boundaries to represent heterogeneous and evolving subsurface terrains [93]. Common clustering and dimensionality-reduction tools include hierarchical clustering for multiscale geological grouping; density-based spatial clustering of applications with noise (DBSCAN) and ordering points to identify the clustering structure (OPTICS) for density-based anomaly detection in irregular data; Gaussian mixture models for probabilistic litho-facies characterization, k-medoids for noise-resilient clustering; principal component analysis (PCA) for feature decorrelation; independent component analysis (ICA) for source isolation; factor analysis for latent structure extraction; and nonlinear manifold learning tools such as t-Distributed Stochastic Neighbor Embedding (t-SNE) and uniform manifold approximation and projection (UMAP) for high-dimensional pattern visualization and structural trend discovery [94,95]. Cluster quality is typically evaluated using internal indices such as Silhouette, Calinski–Harabasz, Davies–Bouldin, Dunn, and S_Dbw, while fuzzy/probabilistic methods employ the Partition Coefficient, Partition Entropy, Xie–Beni, Fuzzy Silhouette, and Kwon indices [96,97]. When partial labels exist, external indices, including Adjusted Rand Index, Normalized Mutual Information, Purity, and Jaccard Similarity, enable benchmarking against known geological or geotechnical classes [98].

AI–EGGE now integrates semi-supervised, self-supervised, hybrid, and physics-informed learning to overcome limited labeled data and improve model generalization. Semi-supervised learning leverages small labeled and large unlabeled datasets through self-training, co-training, and graph-based approaches [87,99]. Self-supervised learning extracts feature representations from unlabeled geophysical data via masked reconstruction and contrastive or patch-prediction tasks [100]. Hybrid workflows combine unsupervised clustering or dimensionality reduction with supervised training to enhance accuracy while preserving geological heterogeneity [25]. Physics-informed learning, including physics-informed machine learning (PIML), physics-informed simple-to-ensemble regressors (PISERs), and physics-informed neural networks (PINNs), embeds governing laws, constitutive relationships, and boundary constraints into model architectures or loss functions to suppress non-physical solutions [100,101], and can be coupled with geostatistics, inversion, and simulation for physical consistency. Model optimization further strengthens AI–EGGE through hyperparameter tuning using Bayesian optimization, evolutionary, and swarm algorithms such as GAs, PSO, differential evolution, Gray Wolf Optimizer (GWO), and hybrid Bayesian optimization–deep learning (BO-DL) strategies for architecture search and loss balancing in physics-informed models [31,100,102]. Together, these approaches deliver more data-efficient, physically consistent,

 doi:10.20944/preprints202605.1511.v1

and scalable AI solutions for subsurface characterization, hazard assessment, and infrastructure resilience.

3.2. Deep Learning Approach

Deep learning (DL), a branch of ML built on multi-layer ANNs, has become a dominant framework for high-dimensional analytics by autonomously learning hierarchical, task-specific features from raw or minimally processed data [103,104]. Its adoption within EGGE continues to expand, improving high-fidelity analysis and prediction across geological and structural feature detection [105], landslide forecasting [106], seismic interpretation [107], groundwater modeling [108], infrastructure monitoring [109], soil and rock classification [13,72], geospatial analytics [110], mineral resource evaluation [111], and environmental impact assessment [112].

Building on the ANN backbone, modern DL increases network depth and architectural complexity to enhance representational capacity, abstraction, and generalization. ANNs provide the foundational neural-network paradigm from which contemporary DL architectures are derived, with advanced models, such as DNNs, CNNs, RNNs, LSTMs, AEs, and deep belief networks (DBNs), representing specialized extensions tailored to spatial, temporal, dimensionality-reduction, and hierarchical feature-learning tasks [105,113,114]. Within EGGE, CNNs and AEs support subsurface imaging, signal refinement, inversion enhancement, and lithological/facies classification [115,116]; RNN/LSTMs model time-dependent deformation, settlement, and slope-movement behavior [117,118]; and DNNs model constitutive behavior, stiffness, and strength for engineering design and risk assessment [119]. Generative and uncertainty-aware architectures, including variational autoencoders (VAEs) and GANs for synthetic data augmentation, scenario simulation, and uncertainty representation, and Bayesian neural networks (BNNs) for probabilistic prediction with quantified epistemic and aleatoric uncertainty, are increasingly enabling more robust and risk-informed decision-making [41,113,117]. DL performance is evaluated using standard ML metrics, alongside training–validation loss dynamics, convergence stability, efficiency, and uncertainty diagnostics for probabilistic and generative models.

3.2.1. ANN Architecture

ANNs are widely used in EGGE for classification and prediction, offering a robust alternative to traditional mathematical formulations for modeling nonlinear soil/rock structure interactions [120,121]. The ANN architecture—an input layer, one or more hidden layers, and an output layer linked by weighted neurons—forms the foundation of modern DL architectures [78]. As shown in Figure 5, ANNs learn nonlinear input–output relationships by adjusting synaptic weights during training, enabling the mapping of geoenvironmental and geotechnical variables (e.g., loading, soil parameters, environmental influences) to mechanical responses. Model complexity, driven by the number of hidden layers and neurons, strongly affects accuracy [122]. A key extension is the Fuzzy Inference System (FIS), which uses fuzzy logic and rule-based reasoning to handle uncertainty in EGGE data [42,123]. Its hybrid evolution, the Adaptive Neuro-Fuzzy Inference System (ANFIS), integrates ANN learning with fuzzy logic for nonlinear modeling with improved interpretability [124]. Another classical variant, the Probabilistic Neural Network (PNN), applies Bayesian decision theory with radial basis activation functions for reliable pattern recognition under uncertainty [125]. ANN training commonly uses Backpropagation Neural Network (BPNN), which updates weights via gradient-based optimization to minimize loss, with optimizers such as Adam and RMSProp improving convergence and generalization [123]. Metaheuristic-based training further reduces error in complex applications [56].

Recent ANN-derived architectures: GNNs for spatial-relational learning, TFs for long-range dependency modeling, and PINNs that embed physical laws, are accelerating a shift toward physics-aware DL [18,39]. This promotes domain-informed, interpretable, and more generalizable models that integrate geoscientific and geotechnical priors. Project DeepGeo [62] exemplifies this by embedding geological knowledge into ANN/DNN workflows through structured training-image

 doi:10.20944/preprints202605.1511.v1

databases for subsurface characterization in data-scarce settings; 54 expert-interpreted cross-sections enabled Bayesian ensemble learning and stratigraphic UQ, demonstrating the value of knowledge-informed DL. Karpatne et al. [126] likewise showed that ANN-based models outperform empirical and statistical approaches by learning latent features governing stress–strain behavior, stiffness, and strength under variable loading and environmental conditions. Despite progress, limitations—data scarcity, spatial bias, overfitting, weak cross-site generalization, and black-box opacity—still hinder large-scale EGGE deployment. Emerging solutions integrate XAI (e.g., SHAP, LIME, Gradient-weighted Class Activation Mapping [Grad-CAM], uncertainty-aware learning, hybrid physics-informed models, and attention-based architectures to improve reliability, transparency, and engineering adoption. Table 1 further summarizes selected reviews and research on ANN applications.

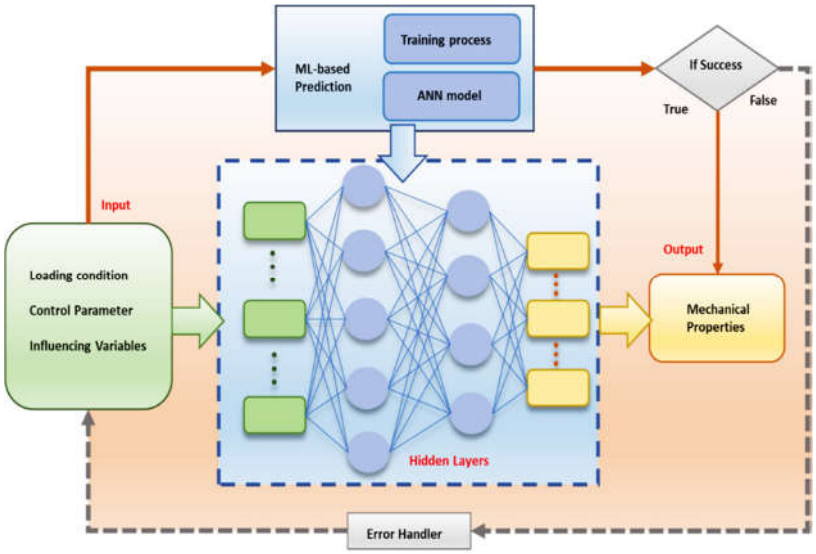

Figure 5. Typical ANN framework for DL–based prediction of geomechanical properties (after [127]).

Table 1. Summary of selected reviews and research on ANN with its variants in EGGE.

Authors	Methods used	Results	Relevance	Limitations
[128]	Time Delay Neural Networks (TDNNs) applied to cyclic swelling data from the powerhouse cavern (Iran)	TDNN successfully modeled cyclic swelling pressure with good accuracy, capturing time-dependent behavior	Demonstrates ANN capability in modeling cyclic swelling/shrinkage of weak rocks (mudrock), critical for underground structures	Dependent on site-specific data, generalizability to other rock formations is uncertain
[129]	ANN (MLP, RBF) and multivariate regression with multivariate non-linear regression (MLR, MNR) to predict shear	MLP-ANN outperformed RBF-ANN; MLR outperformed nonlinear regression; ANN captured complex nonlinear soil behavior	Demonstrated ANN's accuracy in predicting soil cohesion and friction angle using soil index properties	Limited dataset (200 samples); model performance dependent on input combinations

 doi:10.20944/preprints202605.1511.v1

	strength parameters in part of Iran			
[123]	Review of ANN modeling and application issues	Outlined ANN architectures: BPNN, RNN, PNN, and SOM. Input selection, training/testing, and data preprocessing highlighted practical examples in liquefaction, pile capacity, soil classification, and slope stability	Provides a methodological framework for applying ANNs in geotechnical engineering	Issues: network geometry selection, data division, overfitting, computational demands
[24]	Review of AI optimization techniques (ANN, Fuzzy Logic, GEP, ANFIS, GA, etc.) in geotechnical applications	AI methods shown to improve prediction of soil behavior, pile capacity, swelling potential, foundation settlement, liquefaction, and more	Comprehensive overview showing how AI enhances geotechnical modeling, sustainability, and precision	Review article—no new experimental validation; heavy reliance on secondary data
[130]	Bootstrapping DL-ANN with airborne EM and borehole data for saltwater investigation in the Mississippi River Valley (USA)	Developed resistivity-to-lithology and resistivity-to-concentration models, while DL-ANN estimated the total dissolved solute	Results indicate salinity upconing due to excessive pumping	Reliance on used water quality data for training and validating the DL-ANN model. Inherent uncertainties with the transformation of resistivity values to lithologies and chloride concentrations
[131]	Review of ANNs in soil science	ANNs prove to be effective in predicting soil properties (pH, organic carbon, clay content, permeability, compaction, shear	Highlights ANN potential for soil modeling, land-use planning, and precision agriculture;	Review only; lacks detailed experimental validation; applications are mostly limited

 doi:10.20944/preprints202605.1511.v1

strength); useful for soil classification, fertility assessment, erosion prediction, and moisture estimation	relevant to geotechnical behavior predictions	to soil	to the soil science context

3.2.2. Convolutional Neural Networks (CNNs)

CNNs are a leading DL architecture inspired by the visual cortex and widely applied in EGGE for spatial feature learning, enabling automatic multiscale pattern extraction from raw geospatial, geophysical, and imagery data [117]. As shown in Figure 6a–b, a typical AI–EGGE CNN workflow includes data preprocessing, augmentation, and transfer learning using pretrained models such as AlexNet, GoogLeNet, Inception, ResNet, U-Net, and DenseNet to enhance feature extraction and reduce training time and data needs. A standard CNN comprises convolutional and pooling layers with activation functions (e.g., ReLU), followed by either a flatten layer or global average pooling (GAP) before dense layers and a Softmax classifier, with Flatten adopted in Figure 6b. Flatten increases trainable parameters, whereas GAP reduces complexity and mitigates overfitting—beneficial in EGGE where labeled data are limited and heterogeneous [10,13].

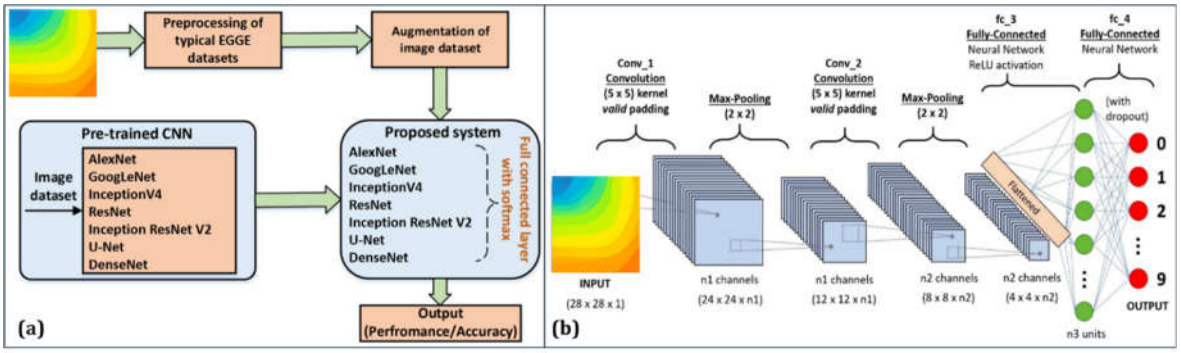

Figure 6. CNN framework for AI–EGGE: (a) workflow integrating preprocessing, augmentation, and pretrained CNN models (AlexNet, GoogLeNet, Inception, ResNet variants), and (b) representative architecture with convolution, pooling, flatten, and fully connected layers for image-based classification.

CNNs outperform traditional ML methods based on handcrafted features by enabling end-to-end, noise-resilient representation learning [104,116]. Performance has been further enhanced through variants such as Visual Geometry Group (VGG), ResNet, and DenseNet for deep residual feature extraction [99,132]; Inception/GoogLeNet and EfficientNet for multiscale and computation-efficient learning [133]; MobileNet for lightweight deployment [106]; 3D-CNNs for volumetric subsurface data [134]; and U-Net, fully convolutional network (FCN), and SegNet for pixel-level segmentation [19,110]. Model evaluation typically uses accuracy, precision, recall, F1-score, and confusion matrices [13], while segmentation and generative CNNs additionally employ Intersection over Union (IoU), dice coefficient, peak signal-to-noise ratio, and Structural Similarity Index Measure (SSIM) [40,135]. High annotation needs, compute cost, and low interpretability are driving progress in transfer learning, few-shot learning, lightweight CNNs, and XAI/physics-informed CNNs [134,136].

CNNs show strong versatility across EGGE for material characterization, geospatial mapping, hazard assessment, and infrastructure monitoring. They routinely achieve >95–99% accuracy in soil and rock classification, texture analysis, and mineral discrimination using core, thin-section, UAV, and hyperspectral imagery [137,138]. Hemdan and Al-Atroush [127] demonstrated that CNN-based

 doi:10.20944/preprints202605.1511.v1

feature extraction combined with SVM improves soil-image recognition accuracy while reducing training cost. U-Net, SegNet, and FCN enable high-resolution segmentation of lithological boundaries and soil horizons, supporting digital soil mapping, fertility and pH assessment, and large-area soil property prediction [139,140]. In remote sensing, CNNs applied to ASTER, Landsat, Sentinel, and UAV data enhance lithological mapping, alteration detection, and landslide susceptibility analysis for early warning and resilience planning [111,141]. CNNs also deliver automated, high-accuracy crack and defect detection in tunnels, retaining walls, pavements, and embankments, outperforming manual inspection and traditional computer vision [142,143]. Hybrid CNN–LSTM/RNN models fuse spatial and temporal learning for slope-movement forecasting, deformation monitoring, and tunnel boring machine (TBM) ground-type recognition, with ResNet-18 and GoogLeNet reporting >96% accuracy for real-time TBM operations [54,133]. Compared with handcrafted image-processing techniques, CNNs provide superior multilevel feature learning and robust end-to-end classification; for instance, ResNet50 and VGG16 exceeded 98% accuracy in soil-aggregate classification [137], and 3D-CNNs delivered very high accuracy for hyperspectral soil imaging [144].

Despite the rapid progress, key gaps persist: cross-site generalization, label imbalance, and domain-shift sensitivity limit deployment, particularly in data-scarce or region-specific studies [13,145]. Emerging solutions include multimodal CNNs integrating geophysical, remote-sensing, and geotechnical imagery; CNN–TF hybrids for long-range spatial dependency learning; and physics-informed CNNs that embed geoscience constraints to suppress non-physical outputs [41,79]. Research is also advancing toward self-supervised and few-shot learning, synthetic data augmentation, and explainable CNNs to reduce labeling burden, improve robustness, and accelerate engineering adoption.

3.2.3. Recurrent Neural Networks (RNNs)

RNNs are DL architectures designed for sequential data, maintaining a hidden state that evolves over time to learn temporal dependencies between observations, an advantage over feedforward and CNN models, which process inputs independently or within finite receptive fields [117,144]. As shown in Figure 7 and expressed in Equations (1) and (2), each input x_t is combined with the previous hidden state h_{t-1} to produce an updated state h_t [146], enabling RNNs to retain temporal memory essential for modeling evolving subsurface and geo-infrastructure behavior. This capability has driven their adoption in EGGE applications involving time-varying responses, including time-lapse geophysics, seismic site-response monitoring, pore-pressure and settlement prediction, slope-stability early warning from sensor streams, and tunnel and embankment health monitoring [147]. Practical deployment requires sequence normalization, handling irregular sampling, and managing concept drift in long-term monitoring [148,149]. To overcome vanishing and exploding gradients, gated variants such as LSTMs and Gated Recurrent Units (GRUs) enable long-range dependency learning and have become the dominant RNN models for sequential geotechnical data [73,150]. Despite their strengths, RNNs struggle with long-sequence cost, noise sensitivity, data drift, limited interpretability, and weak cross-site generalization. These limitations are driving advances such as hybrid CNN–RNNs, multimodal and self-supervised sequence models, and physics-informed RNNs for more robust engineering use. Their performance is typically assessed using time-series metrics (MSE, RMSE, MAE, MAPE) and correlation-based indices.

$$h_t = f(W_{xh}x_t + W_{hh}h_{t-1} + b) \quad (1)$$

$$o_t = g(W_{ho}h_t + c) \quad (2)$$

3.2.4. Deep RNN (DRNNs)

DRNNs extend conventional RNNs by stacking multiple recurrent layers to strengthen temporal feature learning and improve predictive accuracy [24,89,114]. In a typical DRNN architecture, inputs pass through successive RNN/LSTM/GRU layers, with hidden states propagated across time, enabling hierarchical learning of temporal patterns: lower layers capture short-term dynamics, while

 doi:10.20944/preprints202605.1511.v1

upper layers extract long-range and more abstract dependencies [149]. This depth advantage makes DRNNs well-suited for environmental and geotechnical problems involving nonlinear, multivariate time-series behavior. Applications include modeling rainfall–pore-pressure–suction interactions for slope-stability assessment, forecasting ground settlement under cyclic or construction loading, and fusing multi-sensor data for condition monitoring of tunnels, dams, and embankments [149,151]. By capturing both immediate and long-term dependencies in evolving geotechnical signals, DRNNs provide a more reliable basis for time-series prediction, early-warning analytics, and risk-informed geotechnical management.

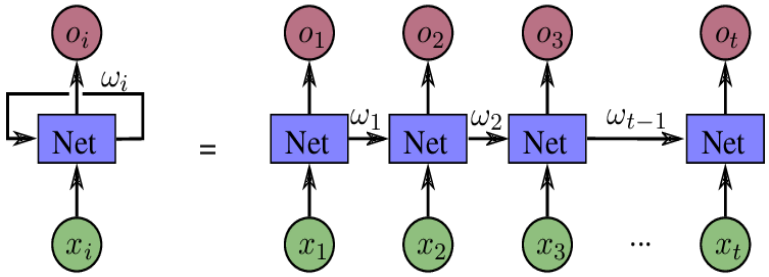

Figure 7. The standard RNN and unfolded RNN (adapted from [146]).

3.2.5. RNN–Autoencoder (RNN–AE) and Bidirectional RNN (BiRNN)

In a typical RNN–Autoencoder (RNN–AE), the encoder compresses multivariate time-series into a latent vector that captures short- and long-term temporal dependencies, and the decoder reconstructs or forecasts sequences from this latent state [24,152]. RNN–AEs integrate the sequential learning ability of LSTM/GRU-based recurrent networks with the feature-learning and dimensionality-reduction strengths of autoencoders, enabling unsupervised representation learning from time-series data [149,153]. For example, the architecture described by Yu et al. [154] and Santoso et al. [153] stacks LSTM/GRU layers for encoding, applies a "RepeatVector" to expand the latent state to the forecast horizon, and employs a mirrored LSTM/GRU decoder with a "TimeDistributed" dense head for output generation. Model capacity is governed by hyperparameters N_1, N_2, and N_3 (units per layer), while dropout and layer normalization enhance training stability and generalization. Training is conducted using a composite loss that combines reconstruction mean squared error (MSE) with multi-step forecasting losses (MSE/MAE), enabling denoising, gap-filling, anomaly detection through reconstruction error, and multi-step nowcasting.

The other variant, Bidirectional RNNs (BiRNNs), processes sequences in both temporal directions to enhance prediction accuracy [149], by employing forward and backward hidden states that capture past and future inputs concurrently, with the outputs merged in a shared layer [114]. This dual perspective alleviates vanishing-gradient limitations and improves context awareness, making BiRNNs particularly effective for sequential learning tasks [133]. These capabilities make RNN–AEs and BiRNNs well-suited to EGGE applications involving noisy, irregular, and multivariate monitoring data, including time-lapse ERT/IP, pore-pressure and settlement logs, rainfall–infiltration–pore-pressure responses, geophysical monitoring, infrastructure-health sensing, and early-warning prediction in geophysical–geotechnical systems.

3.2.6. Gated Recurrent Unit (GRU)

GRUs are an advanced RNN variant for efficient time-series modeling, using gating mechanisms to retain relevant historical information while mitigating vanishing-gradient issues [114]. A GRU cell uses two gates—update and reset—to regulate information flow: the update gate controls how much past state is retained, while the reset gate determines how new input is combined with previous memory. Compared with LSTMs, which use three gates, GRUs have a simpler architecture with fewer parameters, enabling faster training and lower computational cost with minimal accuracy loss [155].

 doi:10.20944/preprints202605.1511.v1

This parsimony makes GRUs suitable for real-time or resource-constrained EGGE workflows involving sensor-based monitoring, dynamic responses, and short- to medium-term forecasting. However, reduced gating complexity can limit long-term dependency modeling, where LSTMs often perform better. Overall, GRUs offer an effective balance of accuracy and efficiency, with the GRU–LSTM choice depending on length, data characteristics, and computational constraints.

3.2.7. Long Short-Term Memory (LSTM)

LSTM networks are an advanced RNN architecture designed to capture long-range temporal dependencies and overcome vanishing-gradient limitations in standard RNNs [112,118,156]. It addresses the problem of the backpropagated error either blowing up or decaying exponentially for long time lags in conventional RNNs. An LSTM cell maintains an internal cell state c_t regulated by three gating mechanisms—input (i_t), forget (f_t), and output (o_t) gates—which control how information is written, retained, and retrieved over time [117] (Figure 8). This gated structure stabilizes the cell state and enables selective preservation of relevant patterns, allowing LSTMs to model long-term sequential behavior more effectively than traditional RNNs and earlier models such as Hidden Markov Models [157,158]. LSTMs are particularly valuable for dynamic processes, e.g., rainfall–infiltration–suction cycles, pore-pressure and settlement evolution, structural health trends, etc., where retaining long temporal context improves forecasting accuracy [114]. However, under irregular or non-uniform time steps, simpler RNN variants may occasionally outperform LSTMs [133]. As shown in Figure 8, an LSTM cell receives the current input x_t and previous hidden state h_{t-1}, which pass through the forget, input, and output sigmoid gates, as well as a candidate state generated via a $tanh$ activation. The cell state is updated as (Equation (3)):

$$c_t = f_t \odot c_{t-1} + i_t \odot \tilde{c}_t, \quad (3)$$

while the hidden output is computed as (Equation (4)):

$$h_t = o_t \odot \tanh(c_t) \quad (4)$$

The gated memory pathway preserves gradients across long sequences, enabling stable training and reliable multi-step forecasting in noisy, nonlinear EGGE time-series data. Building on this capability, Bidirectional LSTM (BiLSTM) and Bidirectional GRU (BiGRU) extend the architecture by processing sequences in both forward and backward directions, allowing the model to learn from past and future context simultaneously [89]. At each time step, BiRNNs generate forward and backward hidden states that are fused to produce a context-enriched representation, particularly advantageous when complete sequences are available prior to inference, and when delayed outcomes depend on earlier and later events within the time window [133,154]. In EGGE, BiLSTM/BiGRU models have demonstrated superior performance compared to unidirectional variants by capturing fuller temporal dependencies in geotechnical signals, improving forecasting accuracy for slope-failure precursors, settlement evolution, seismic site response, TBM-induced vibrations, and structural-health trends in buried and surface infrastructure [133,149,159].

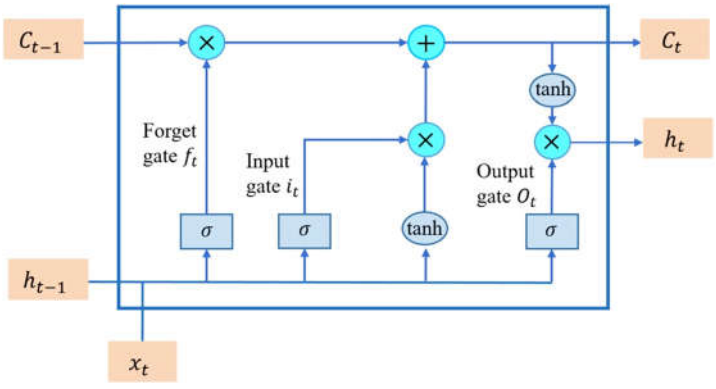

Figure 8. LSTM architecture (adapted from [117]).

 doi:10.20944/preprints202605.1511.v1

3.2.8. Generative Adversarial Networks (GANs)

GANs, introduced by Goodfellow et al. [160], are a key DL architecture for generative modeling. A GAN trains a generator G to produce synthetic samples and a discriminator D to distinguish them from real data through an adversarial minimax process [117], Figure 9a. Originally for unsupervised learning, GANs now support semi-supervised, supervised, and reinforcement learning, enabling data synthesis, super-resolution, domain translation, and anomaly detection [161,162]. Several variants enhance stability and performance: Deep Convolutional GAN (DCGAN) improves image quality using convolutional blocks; Wasserstein GAN (WGAN) stabilizes training and reduces mode collapse; Auxiliary Classifier GAN (ACGAN) enables label-conditioned generation; Variational Autoencoder GAN (VAE-GAN) fuses latent regularization with adversarial learning for sharper samples; Conditional GAN (cGAN) incorporates auxiliary data (e.g., lithology); CycleGAN performs unpaired image-to-image translation; and PatchGAN evaluates local patches to enhance fine-scale texture and spatial detail [30,161].

In EGGE, GANs help overcome data scarcity, improve model generalization, and enhance subsurface characterization. Key applications (Table 2) include synthetic augmentation of soil/rock datasets, reconstruction of incomplete borehole, seismic, and monitoring time series, pore-scale microstructure generation, and super-resolution of seismic and GPR imagery. Conditional and cycle-based GANs also enable cross-domain mapping (e.g., geophysical-to-lithology translation) [163]. Challenges persist—training instability, mode collapse, computational cost, and validation—but GANs remain promising for data enrichment, geo-imaging enhancement, and inversion and simulation support [30,164]. To address some of these limitations, Yan et al. [165] integrate CycleGAN-based cross-modal enhancement with hierarchical feature fusion to improve multi-sensor image integration (e.g., Vis–SAR) (Figure 9b), marking a shift toward reducing modality gaps and improving fusion consistency for high-fidelity geo-imaging.

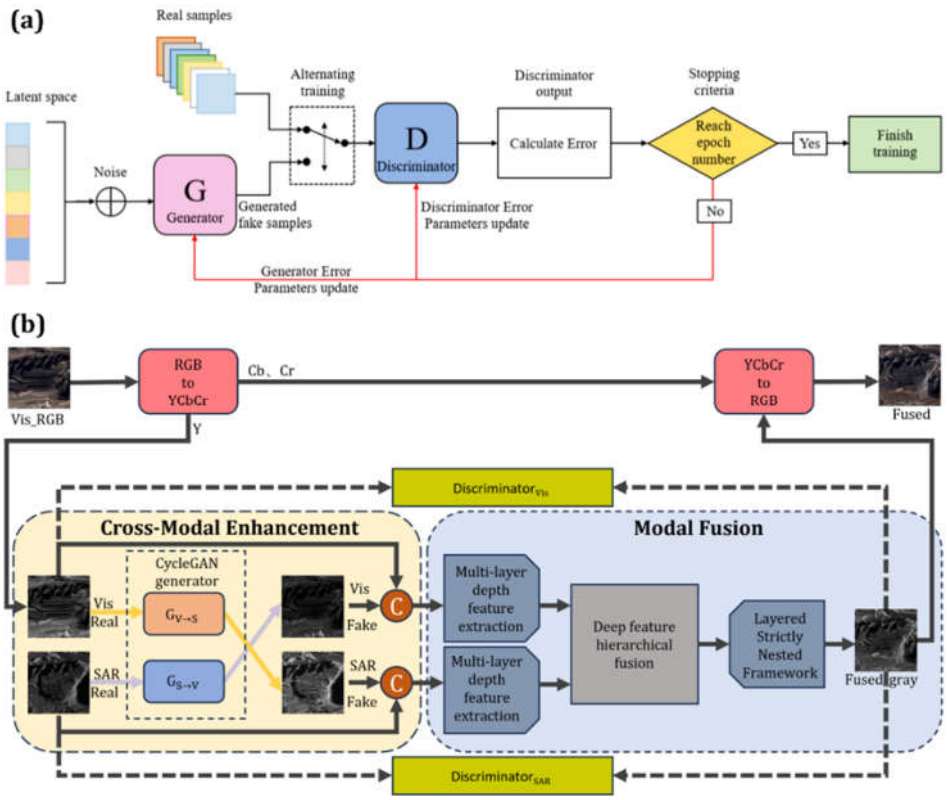

Figure 9. (a) Schematic diagram of the GAN (adapted from [117]. (b) Typical advanced GAN-based cross-modal fusion framework integrating CycleGAN-driven cross-modal enhancement with hierarchical deep feature

 doi:10.20944/preprints202605.1511.v1

fusion (adapted from [165]). The model learns bidirectional mappings between visible (Vis) and SAR modalities via generators $G_{V\to S}$ and $G_{S\to V}$, with adversarial feedback from modality-specific discriminators.

Table 2. Summary of selected studies on GAN with its variants and their relevance in EGGE.

Author	Methods used	Results	Relevance	Limitations
[160]	Original GAN framework using generator + discriminator (MLP)	Demonstrated competitive sample generation on MNIST, CIFAR-10, and TFD datasets	Foundational to geotechnical applications (later adopted for soil/rock modeling, subsurface imaging)	Training instability, lack of explicit probability density, and mode collapse
[166]	GANs, cGANs, WGANs; applied to CIFAR-10 and medical images	Augmented datasets improved accuracy (e.g., CIFAR-10: +7.3%; medical imaging: +6.7%); significant FID/IS improvements	Framework directly transferable to geotechnical datasets (soil/rock images, seismic/GPR data)	Training instability, quality control of synthetic data, and high compute costs
[161]	Variants: DCGAN, WGAN, ACGAN, VAE-GAN; review of structural and loss-function improvements	Summarized enhancements that stabilize training & improve diagnostic accuracy	Shows potential of GANs in generating synthetic geotechnical signals (e.g., vibration data for fault diagnosis)	Training instability, domain transferability issues
[167]	Image-to-Image GAN (Pix2Pix) trained on synthetic RF data representing soil layers (sand, silt, clay); Soil behavior type index (Ic) used as input	Achieved mean absolute error (MAE) of 0.039 vs. 0.096 for nearest-neighbor interpolation; accurate for Ic < 3; demonstrated the feasibility of GANs for 2D soil schematization	Provides a novel AI-based approach for subsurface schematization, outperforming traditional interpolation; supports efficient soil classification and modeling with limited data	Based solely on synthetic data; performance biased toward datasets dominated by Ic < 3; requires balanced datasets; validation with real field data still needed
[163]	Multi-scale GAN (MS-GAN) for 3D geological modeling	Generated multiple 3D realizations capturing stratigraphy with quantified uncertainty	Highly relevant for site characterization, 3D subsurface modeling in geotechnics	Computationally intensive; depends on the quality of the training image; irregular

 doi:10.20944/preprints202605.1511.v1

				boreholes require additional processing
[30]	SchemaGAN: cGAN with U-Net generator & PatchGAN discriminator; trained on 24,000 synthetic cross-sections and CPT-like data	Outperformed interpolation methods (MAE ≈ 0.039 vs. 0.096 for nearest-neighbor; better layer boundaries, anisotropy, and complex geometries); validated through blind expert survey and Dutch field case studies	Demonstrated robust, realistic subsurface schematization from sparse CPT data; scalable tool for geotechnical site characterization and digital twin applications	High computational training cost (95h on supercomputer); still reliant on synthetic training data; limited to 2D (needs extension to 3D); may struggle if field conditions deviate from training database

3.3. Physics-Informed Neural Networks (PINNs) in AI–EGGE

PINNs are neural networks that solve partial differential equations (PDEs) by embedding physical laws or other governing constraints directly into the loss function, ensuring physics-consistent learning [168–170]. By converting these constraints into additional loss terms, PINNs integrate observational data with PDE residuals, initial, and boundary conditions to guide training, thereby enhancing generalization, reducing dependence on large labeled datasets, and improving interpretability relative to purely data-driven DL [23,171]. This capability is particularly relevant to EGGE, where subsurface behavior is governed by PDE-based geophysical and geotechnical laws [59,172]. Within the AI–EGGE paradigm, PINNs mark a shift from conventional pattern-recognition DL toward physics-informed learning, enabling models to retain mechanistic fidelity while leveraging data-driven flexibility [39]. Figure 10 illustrates a multi-receptive-field PINN (MRF–PINN) [171]. The initialized input field (u_0) is processed through parallel encoder–decoder branches with different receptive fields ($RF_1 - RF_6$), enabling multi-scale feature extraction. Each branch produces intermediate feature maps ($u_1 - u_6$) and corresponding predictions ($p_1 - p_6$), which are recombined via feature-map aggregation and linear superposition to form the MRF–PINN prediction field. Training is guided by a composite loss function, where weighting coefficients λ_{data}, λ_{BC}, λ_{PDEs}, balance data misfit (L_{data}), boundary-condition constraints (L_{BC}), and physics-based PDE residuals (L_{PDEs}). This design supports stable learning of multi-scale, heterogeneous, and coupled subsurface processes characteristic of EGGE systems, e.g., [11,173].

PINNs have shown strong capability for forward and inverse modeling in EGGE, with applications in soil/rock consolidation [174], groundwater [59], seismic wave propagation [38], subsurface stress distribution [22], tunneling [172], and pile–soil interaction [175]. They deliver physically credible predictions under sparse or imperfect data and achieve accuracy comparable to analytical and numerical solutions, with growing value for parameter inference [138,176]. Ito et al. [177] estimated the coefficient of consolidation for Terzaghi's 1D consolidation and unsaturated hydraulic properties directly from laboratory data. However, widespread adoption remains limited by reliance on synthetic data, reduced robustness under field noise and heterogeneity, training instability, slow convergence, loss-term sensitivity, and difficulty modeling highly nonlinear or coupled hydro-geomechanical processes [22,178,179]. Emerging advances, such as hybrid

 doi:10.20944/preprints202605.1511.v1

architectures (e.g., MRF-PINNs, operator-learning PINNs), adaptive loss balancing, integrated field–lab data training, uncertainty- and XAI-enhanced PINNs, and PINN–numerical solver coupling [171,180], are accelerating the shift toward trustworthy, physics-informed, and field-deployable AI for EGGE, laying the foundation for neural-operator models and real-time digital-twin subsurface systems. For example, Figure 11, Arif et al. [10], integrates an optimum GBM classifier with a PINN for circular slope-stability diagnosis: the GBM is trained on a 221-case dataset (inputs: H/h, slope angle β, cohesion c, unit weight γ, friction angle φ, and pore-water pressure r_u) with 5-fold cross validation (CV), while the PINN enforces physics constraints to regularize learning. This hybrid achieved the strongest F1/κ–AUC performance and outperformed ANN, SVM, and RF baselines, demonstrating how physics guidance enhances generalization under limited data.

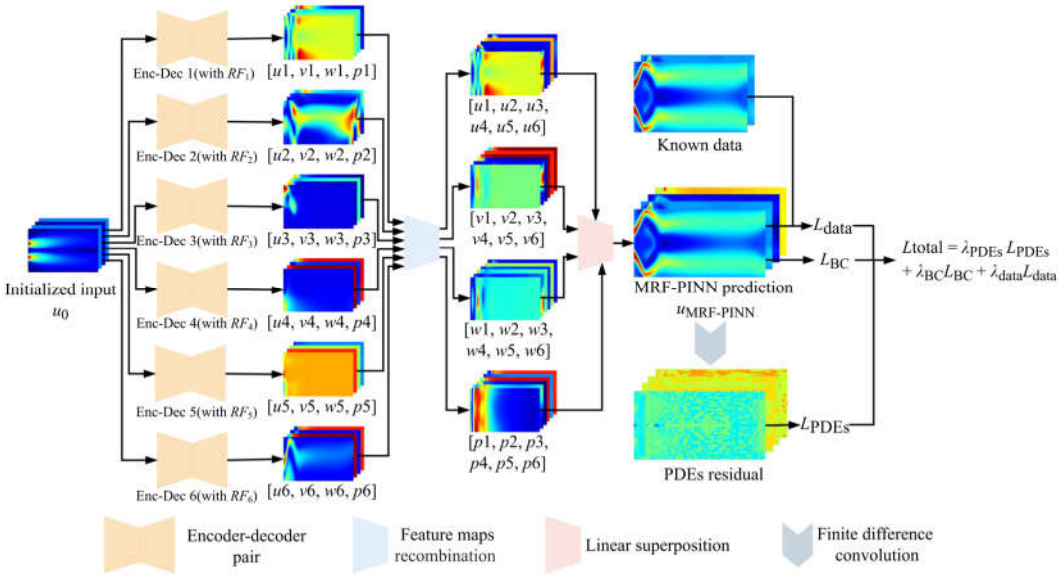

Figure 10. PINN framework with six encoder-decoder pairs for solving PDEs, each assigned a distinct convolutional receptive field [171].

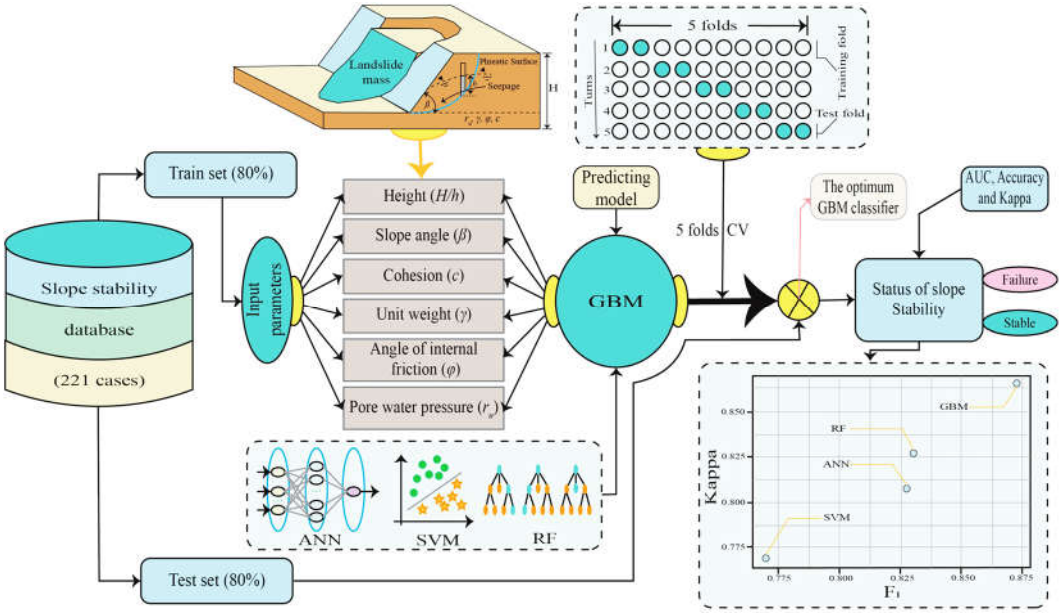

Figure 11. Hybrid GBM with PINN framework for predicting circular slope stability (adapted from [10]).

 doi:10.20944/preprints202605.1511.v1

4. Emerging Trends in AI–EGGE

The increasing complexity and nonlinearity of subsurface systems now require analytical frameworks that can integrate diverse geophysical, geotechnical, remote-sensing, and environmental datasets into unified, physically consistent models. This need is driving a shift in AI–EGGE toward physics-informed, multimodal, explainable, and increasingly autonomous intelligence capable of capturing coupled subsurface processes and supporting real-time decision-making [181,182]. This shift is being enabled by the integration of ML/DL with physics-based modeling, multimodal data fusion, UQ, and edge-intelligent sensing, aimed at improving model reliability, transparency, and operational deployment [183,184]. At the core of this evolution is multimodal fusion, which integrates heterogeneous datasets to reconcile differences in sensitivity, resolution, and noise [4,185], thereby reducing interpretational ambiguity and strengthening predictive robustness for environmental and geotechnical decision-making.

4.1. Explainable AI (XAI): Concept and Model Framework

As AI systems become embedded in geophysical–geotechnical workflows, interpretability is essential for scientific credibility, regulatory acceptance, and geoenvironmental and geoengineering deployment. In XAI, the terms *white-box*, *gray-box*, and *black-box* denote increasing opacity in a model's internal logic and decision-making process [186], influencing model selection in EGGE applications. White-box models are inherently interpretable but often less accurate; gray-box models balance interpretability and performance; and black-box models typically achieve higher accuracy at the expense of transparency. XAI promotes transparency by linking model predictions to physical properties, uncertainty sources, and domain knowledge, converting opaque outputs into defensible analytical insights. It aims to make AI results understandable and trustworthy for both domain specialists and system developers, supporting error diagnosis, model refinement, and responsible use in high-consequence contexts [9,79,186]. XAI methods fall into two groups: intrinsically interpretable models designed for transparency (e.g., EBM, NAM, CBM) and post-hoc techniques that explain complex models (e.g., SHAP, LIME, IG, Grad-CAM, ALE) [187,188]. Beyond transparency, XAI supports scientific consistency by ensuring that learned representations align with physical principles and empirical evidence critical in EGGE, where decisions must withstand scrutiny under partial observability and high impact [189]. Table 3 summarizes the key XAI and uncertainty evaluation methods essential for interpreting multimodal models and assessing their predictive reliability.

Table 3. Summary of XAI and uncertainty evaluation methods.

Category	Method	Full Name	Description	Applications
Post-hoc XAI	SHAP	SHapley Additive exPlanations	Quantifies each feature's contribution (positive or negative) to a prediction using Shapley values	Best for local and global interpretability with strong theoretical grounding
	LIME	Local Interpretable Model-Agnostic Explanations	Generates a simple local surrogate model (often linear) to approximate how features influenced a specific prediction, providing fast, model-agnostic	Useful for explaining individual geotechnical or environmental predictions (e.g.,

 doi:10.20944/preprints202605.1511.v1

			insight into the key drivers of that outcome	why a specific site was classified as high-risk)
	Grad-CAM	Gradient-weighted Class Activation Mapping	Produces gradient-based heatmaps that show which regions of an input image most influenced a model's decision, providing a visual explanation of "where the model looked"	Relevant for seismic/image-based data, landslide mapping, to verify physical/geological focus.
	ALE	Accumulated Local Effects	Shows how a feature affects model predictions on average, accounting for feature interactions without bias from correlated features	Best for global interpretation when features are correlated
	IG	Integrated Gradients	Computes feature attributions by integrating model gradients from a baseline input to the actual input.	Best for interpreting DNNs with continuous features.
Intrinsic (Ante-Hoc) Models	EBM	Explainable Boosting Machine	A glass-box boosted GAM (Generalized Additive Models) that learns interpretable features and interaction effects	When high accuracy + full transparency are required for tabular geoscience data
	NAM	Neural Additive Model	A neural form of GAMs where each feature has its own subnetwork, preserving additive interpretability	When nonlinear patterns require neural network flexibility without sacrificing interpretability
	CBM	Concept Bottleneck Model	Predicts human-defined concepts first, then uses them for the final prediction, enforcing semantic reasoning	When explanations must align with domain concepts (e.g., soil type → stiffness → failure risk)
Uncertainty & Performance Metrics	PI	Prediction Intervals	Provide an estimated range within which the true value is expected to lie at a given confidence level.	Quantifies predictive uncertainty for risk-aware decision-making.

 doi:10.20944/preprints202605.1511.v1

Coverage	PI Coverage	Percentage of observed values falling within the prediction intervals	Evaluates calibration of uncertainty estimates (ideally ≈ target confidence)
CRPS	Continuous Ranked Probability Score	Compares the full predictive distribution with the observation to assess probabilistic accuracy (lower = better).	Measures calibration + sharpness of probabilistic predictions—superior to RMSE for uncertainty models
NRMSE	Normalized Root Mean Squared Error	Scale-independent measure of prediction error normalized by range, mean, or standard deviation (lower = better)	Allows fair model comparison across variables, sites, or units

4.1.1. Post-Hoc Methods

Post-hoc methods explain trained models at local or global levels. Key feature-attribution tools include Integrated Gradients and its refinement, Guided IG, which reduces attribution noise, and Shapley-value methods, with dependence-aware variants preferred when predictors are correlated [188,189]. For global effects, ALE is generally favored over Partial Dependence Plots (PDPs) as it avoids extrapolation under correlation, with recent work improving its efficiency in high-dimensional settings. These methods support factor-effect interpretation in geospatial workflows involving terrain, soil, or geophysical attributes [56]. However, post-hoc explanations may be unstable, inconsistent, or unfaithful to model logic; thus, quantitative tests of faithfulness and stability are recommended over visual inspection alone [81,190]. Demonstrated value in EGGE includes landslide susceptibility modeling, where SHAP-based analyses reveal the influence of slope, precipitation, and lithology, with similar usage in hazard mapping, subsoil classification, and monitoring [80,191].

4.1.2. Intrinsic (Ante-Hoc) Methods

Intrinsic approaches embed interpretability in the model form and are advantageous for validation in safety-critical engineering contexts. Modern additive models include NAMs, which retain GAM-like clarity with neural flexibility, and EBMs, which provide transparent, shape-constrained feature effects with competitive accuracy [180,187]. CBMs introduce human-auditable intermediate concepts to enable inspection and correction at the concept layer [192]. A related direction leverages physics-informed ML (PIML) or physics-guided ML, embedding physical laws, constraints, or forward operators into the architecture or loss to yield predictions interpretable through constraint satisfaction and residuals—useful for inversion and property mapping in EGGE [101,169,180].

4.1.3. Integrated Applications

Applications in EGGE demonstrate the value of XAI for improving model credibility, interpretability, and deployment. For instance, Wang et al. [80] employed an XAI–DL framework to derive global and local insights into hydro-morphological processes (HMP) across China to aid in

 doi:10.20944/preprints202605.1511.v1

hazard and risk assessment, achieving ten-fold cross-validated AUC scores of 0.83–0.86. The SHAP-based interpretations revealed that spatially varying feature contributions to HMP predictions can diagnose model behavior, validate physically meaningful drivers, and support regional-scale environmental analysis. In landslide susceptibility modeling, e.g., [80,188], interpretable neural networks and SHAP-augmented ensembles similarly expose dominant predictors and interactions (e.g., slope–precipitation coupling, lithology, aspect), improving user trust and guiding model refinement. In geotechnical property prediction and soil classification, SHAP, ALE, and partial-dependence diagnostics clarify how CPT-derived indices and soil parameters influence outputs [9,16]. Similarly, Degen et al. [180] show that architectures that embed domain constraints into feature learning enhance classification performance while preserving the interpretability of the physical cues used. Overall, XAI strengthens due diligence in EGGE, supporting sensitivity and scenario analysis, defensible decision-making, and model-risk management across heterogeneous datasets [189].

The practical guidance XAI interpretations include:

1. Use intrinsic models (EBM, NAM, CBM) where interpretability is essential; apply post-hoc methods mainly for auditing, debugging, and communicating complex models, and validate explanations with faithfulness and stability checks.
2. In correlated multimodal settings, favor ALE and dependence-aware SHAP over naïve PDP/SHAP pipelines.
3. Where physical laws are well established, adopt physics-informed hybrids to couple accuracy with mechanistic interpretability and diagnosable residuals.
4. Quantify uncertainty in explanations (e.g., confidence intervals for feature effects or attribution variability across perturbations) to avoid overconfident interpretation in high-stakes EGGE decisions.
5. Communicate explanations at the appropriate level of abstraction for the audience (engineers, regulators, field practitioners), emphasizing actionable insights rather than raw attribution maps.

4.2. Multimodal Fusion: Concept, Hierarchy, Strategies, and Methodological Approaches

Multimodal fusion in AI–EGGE refers to the systematic integration of heterogeneous datasets to achieve a more complete, reliable, and physically consistent representation of subsurface and engineered environments [4,193]. The conceptual hierarchy of multimodal fusion spans three integration levels: low-, mid-, and high-level fusion. Low-level (data-level) fusion combines raw or minimally processed datasets to preserve intrinsic spatial and physical relationships; mid-level (feature-level) fusion generates shared latent representations by combining engineered or learned features to improve discrimination of lithological boundaries, hydrostratigraphic units, geomechanical heterogeneities, and deformation precursors; and high-level (decision-level) fusion aggregates outputs from independently trained models through ensemble learning, Bayesian model averaging, and probabilistic late-fusion schemes to strengthen robustness, interpretability, and out-of-distribution generalization [4,21,182,183,194]. This conceptual multimodal fusion framework is illustrated in Figure 12, summarizing the flow from data acquisition and preprocessing through fusion levels and AI modeling to interpretability, uncertainty assessment, and end-use applications.

Relevant data sources include geophysical surveys (resistivity, seismic, GPR, magnetic, gravity), geotechnical investigations (borehole logs, SPT-N, CPT-qc, laboratory tests), and remote-sensing and environmental observations such as UAV imagery, light detection and ranging (LiDAR), synthetic aperture radar (SAR), interferometric SAR (InSAR), and soil chemistry. Each modality contributes distinct yet complementary strengths: geophysical methods provide broad spatial coverage but often suffer from non-uniqueness and depth-resolution limitations, whereas geotechnical data offer high-fidelity ground truth but are spatially sparse. Their fusion reduces interpretational ambiguity, tightens model uncertainty, and enhances the effective spatial resolution and structural interpretability of subsurface models for geoenvironmental and geoengineering decision-making

 doi:10.20944/preprints202605.1511.v1

[193,195,196]. Table 4 provides a complementary overview focusing specifically on the hierarchy of fusion levels, representative techniques, and computational enablers adopted in EGGE.

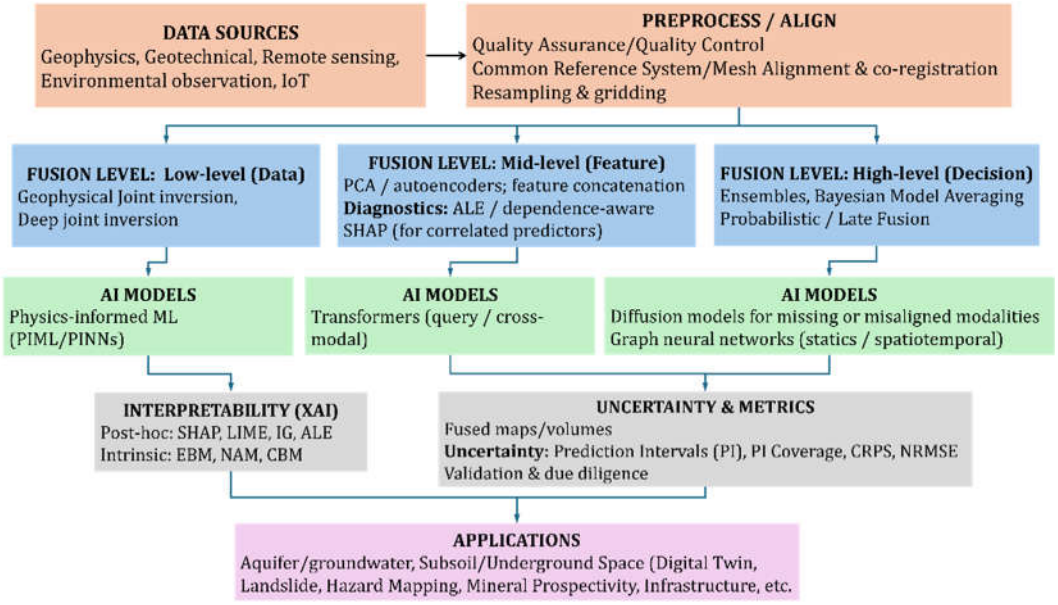

Figure 12. Multimodal fusion framework in AI–EGGE, outlining the workflow from data source and preprocessing through fusion levels, AI modeling, interpretability, and uncertainty analysis to final applications.

Table 4. Conceptual hierarchy of multimodal fusion levels and representative methods in EGGE.

Level	Definition	Representation	EGGE Examples	References
Low level (data)	Fuse raw/minimally processed observations (joint inversion) to mitigate non-uniqueness and depth-resolution trade-offs	Joint inversion (DC–TEM, TEM–RMT (radio-magnetotelluric), DC–Gravity); deep joint inversion with U-Net reparameterization	DC–TEM (transient electromagnetic) joint inversion; TEM–RMT joint inversion; physics-constrained Swin Transformer for gravity inversion	[182,183,193, 197]
Mid-level (feature)	Fuse engineered/learned features via statistics/ML; handles heterogeneous geophysical/geotechnical/monitoring data	PCA/ALE, AEs; feature concatenation; intermediate-fusion deep nets	Excavated soil classification (images + CPT + TDR); underground mining geo-hazards (multimodal)	[181–183]
High-level	Fuse model outputs/decisions (ensembles, probabilistic combination) to	Stacking/ensembles; Bayesian model averaging; conformal risk control for UQ	Ensembling susceptibility maps; combining geophysics-only and fused models for risk	[165,182]

 doi:10.20944/preprints202605.1511.v1

	improve robustness and UQ		scoring with calibrated UQ	
Advanced AI frameworks (EGGE-adjacent)	Flexible multimodal fusion and missing/misaligned modality handling	TF (Geometric Query); physics-constrained TF; spatiotemporal GNN; diffusion models for missing modalities/completion	Multimodal geophysical inversion (TF); gravity inversion (Swin-TF); structural sensing fusion (GNN); EMAG2 gap-fill & multi-view completion (diffusion)	[40,184,185]

Methodologically, multimodal integration in EGGE is enabled through five overarching strategy classes: physics-governed fusion (e.g., joint and cooperative inversion) that embeds physical constraints; data-driven fusion using ML/DL architectures; hybrid physics–AI fusion that couples domain knowledge with learning-based models; cross-modal alignment strategies that learn shared latent spaces for correlated modalities; and probabilistic and uncertainty-aware fusion to quantify confidence and support risk-informed decision-making [45,182]. Recent advances further incorporate AI-driven approaches, including physics-informed ML (PIML/PINNs) for physics-consistent multimodal learning, transformer-based and contrastive cross-modal fusion for spatial-temporal representation alignment, diffusion and GAN models to infer or reconstruct missing modalities, and GNN- and spatiotemporal fusion frameworks for continuous deformation assessment, infrastructure monitoring, and hazard early warning [165,185,194]. Deep attention-enhanced fusion architectures are also emerging, exemplified by Yan et al. [165], who integrate multi-layer deep feature extraction, hierarchical feature fusion with attention, and a Layered Strictly Nested Framework (LSNF) to achieve robust SAR–visible image fusion with preserved structural integrity and high-frequency detail. Recent evidence shows that integrating borehole and laboratory data with ground and airborne geophysics sharpens hydrostratigraphic and deformation models and strengthens prediction in EGGE [195,196]. Physics-consistent joint inversion further improves structural coherence in integrated subsurface interpretation [193,198]. Remote-sensing fusion (optical/SAR/LiDAR) adds terrain, deformation, and environmental constraints at scale, supporting hazard-prone and urban-infrastructure applications [4,64,199].

5. Applications and Case Studies of AI–EGGE

5.1. Applications

The practical deployment of AI–EGGE has advanced from isolated algorithmic trials to robust, field-validated decision-support systems. Beyond conventional supervised and unsupervised ML, recent developments integrate DL architectures, physics-informed and mechanistic modeling, multimodal and cross-domain data fusion, and XAI to enhance trust, interpretability, and engineering uptake. These advances now enable high-resolution subsurface characterization, soil and lithological classification, geotechnical parameter prediction, groundwater assessment, geohazard forecasting, underground infrastructure monitoring, and real-time sensing for resilient engineering design. This section presents application cases demonstrating how AI–EGGE is transforming data acquisition, interpretation, and risk-informed decision-making across environmental and engineering contexts.

 doi:10.20944/preprints202605.1511.v1

5.1.1. Site Characterization and Subsurface Profiling

AI–EGGE strengthens site characterization by improving assessment of soil–rock interactions and subsurface conditions, reducing trial-and-error investigations. It enables reliable prediction of groundwater levels, soil texture, particle-size fractions, organic carbon, pore-water pressure, and soil movement, lowering exploration costs and improving design efficiency. Accurate subsurface characterization is critical because physical, mechanical, and hydraulic properties govern structural performance [6,14,87]. Compaction, shear strength, and permeability control foundation support, while interactions—such as water content, viscosity, and earth pressure in clays—affect strength and deformation. Data-driven and statistical methods enhance characterization by revealing patterns often missed by conventional approaches.

ML models have been widely applied to estimate soil hydraulic properties [100,200], soil organic carbon and matter [201], and soil pore structures [53,77]. Notable examples include ANNs and the Group Method of Data Handling (GMDH), a self-organizing polynomial-based ML method, which have provided deeper insight into site properties [75,108,202]. Licznar and Nearing [203] applied ANNs to predict hydraulic behavior, and Mishra et al. [204] used RF and SVM to estimate bulk density and cation exchange capacity at different depths. Extreme learning machine (ELM), RBF, modified GMDH, and M5 tree methods have proven effective for predicting pore-water pressure, groundwater table elevation, and soil-water retention curves (SWRC), which are central to hydrological processes and soil moisture dynamics, and agro-hydrology [205]. A wide range of soil attributes—from texture and organic matter to hydraulic and retention properties—serve as key inputs for ML-based SWRC estimation. ANN- and DNN-based models have also been used to predict soil temperature [42,206].

Despite advances, site-specific soil and rock heterogeneity still necessitate complementary laboratory testing. Consistently with this, Wang et al. [207] assessed RF, SVM, gradient-boosted regression trees, MLP, and least angle regression (LAR) for hyperspectral-based soil salinity prediction, with LAR showing superior stability and accuracy. Elaziz et al. [208] also applied XGBoost, RF, and GBM to 120 soil samples for predicting soil salinity in semi-arid regions, with a success rate between 0.99% to 1.0%. Zhang et al. [209] reported that XGBoost achieved the highest accuracy for total soil nitrogen prediction, RF performed best with SAR data, and GBM outperformed other models when using Landsat-8 and Sentinel-2 data compared to Sentinel-1. These highlight the value of integrating ML with multisource satellite data for precise soil nutrient mapping and improved geotechnical prediction, risk assessment, design optimization, and decision-making. Table 5 provides additional AI–EGGE studies on soil prediction and classification.

Table 5. Selected research on the applications of AI for site characterization and soil–structure prediction.

Authors	Methods used	Results	Relevance	Limitations
[137]	Applied deep CNN models (ResNet50, VGG16 (Visual Geometry Group Network), InceptionV3) to classify soil aggregate sizes from digital images; the dataset contained soil	Achieved high classification accuracy: ResNet50 (98.7%), VGG16 (97.9%), InceptionV3 (97.5%). Demonstrated strong generalization across aggregate size categories	Provides robust, automated classification of soil aggregates, which is vital for assessing soil structure, stability, and compaction relevant to geotechnical and environmental engineering	Limited dataset diversity (lab-prepared aggregates); requires extension to field conditions; performance may decline for highly heterogeneous soil samples

 doi:10.20944/preprints202605.1511.v1

	aggregates of varying classes			
[90]	Smartphone-based imaging system + CNN & RF; 90 soil samples from India (sand to clay). Features extracted: color, local, and texture	High accuracy: Clay (R^2 = 0.97–0.98), Sand (R^2 = 0.96–0.98), moderate for Silt (R^2 = 0.62–0.75). Developed an Android app for soil texture prediction	Enables low-cost, portable soil classification, useful for field geotechnical surveys where rapid soil assessment is needed	Moderate accuracy for silt; model is sensitive to soil moisture and organic matter; requires controlled image capture
[133]	Field TBM vibration data; CNNs (GoogLeNet, ResNet) & RNNs (LSTM, BiLSTM); wavelet-based features	CNN (ResNet-18) achieved 98.28% accuracy, and is superior to RNN (≈80%)	Real-time ground condition identification during tunneling—crucial for TBM safety and efficiency	Relies on site-specific vibration datasets; generalizability to different geologic terrains is uncertain
[143]	Deep learning (CNN with VGG), preprocessing (grayscale, thresholding, edge detection), 40,000 RGB images	Achieved very high accuracy (F1 ≈ 99.5%); grayscale models performed similarly to RGB, edge/thresholding slightly worse	Enables automated, reliable, fast crack detection in concrete infrastructure (bridges, pavements, buildings)	Limited study on real-world noisy/low-quality images; controlled dataset
[210]	CNN and six DCNNs (ResNet, VGGs, Inception-ResNetV2, Xception, DenseNet) on 903 soil images	CNN achieved 99.86% (train) and 97.68% (validation); ResNet: 99.15%; other DCNNs >97%	Validates CNN/DCNNs for soil classification in geotechnical and agricultural domains	Limited datasets and soil types (alluvial, black, clay, red); generalizability uncertain
[211]	Developed lightweight CNN models for soil image classification; compared performance with standard CNNs; dataset of soil	Lightweight CNN achieved comparable accuracy to deeper CNNs (~95–98%) with reduced computational demand; improved	Provides efficient soil classification models suitable for geotechnical site surveys where rapid, on-site predictions are needed, especially	Dataset size and diversity are limited; generalization across soil types and field conditions requires further

 doi:10.20944/preprints202605.1511.v1

	images used for training/validation.	efficiency for real-time use	with limited hardware resources.	validation; performance for complex textures (e.g., mixed soils) has not been fully tested.
[99]	Rapid and accurate prediction of soil texture using an image-based deep learning autoencoder convolutional neural network random forest (DLAE-CNN-RF) algorithm	Developed a smartphone-based image acquisition system; extracted particle, color, and texture features; applied a hybrid DLAE-CNN-RF algorithm for soil texture prediction.	Achieved very high prediction accuracy: sand (R^2 = 0.99), Clay (R^2 = 0.98), silt (R^2 = 0.98). Outperformed KNN and VGG16-RF. Designed a GUI for practical soil texture prediction	Provides a low-cost, portable, and efficient alternative to conventional soil texture analysis, enabling rapid characterization crucial for soil mechanics and geotechnical site investigation
[140]	ML algorithms: SVM, DT, RF, XGBoost, KNN, applied to NPK, soil pH, rainfall, temp, humidity dataset (2100 samples)	XGBoost achieved the highest accuracy: Crops (99.09%), horticultural crops (99.3%), and the combined model (98.51%). Demonstrated crop-specific modeling improves accuracy	Highlights the potential of ML for soil fertility and crop suitability, relevant for optimizing soil-crop interactions and improving site-specific soil use	Focused on agriculture; indirect link to geotechnical engineering. Requires large curated datasets; may not generalize to all soil types
[2]	Custom lightweight CNN (Light-SoilNet), dataset of 392 soil samples (sieve + hydrometer verified), smartphone images	Accuracy 97.2% across 5 soil classes (sand, clay, loam, loamy sand, sandy loam)	Low-cost soil classification tool for geotechnical surveys in agriculture & construction	Small dataset; only 5 soil classes; imbalanced dataset handling needed
[138]	Hybrid CNN–TF with Gate-Shift-Fuse for hyperspectral imaging	Achieved state-of-the-art accuracy (up to 99.86%) on benchmark HSI datasets; superior feature fusion and robustness	Relevant to soil mapping, mineral exploration, and subsurface geotechnics via hyperspectral remote sensing	Computationally intensive; fixed patch sizes; generalization across diverse datasets is uncertain

 doi:10.20944/preprints202605.1511.v1

5.1.2. Landslides

Landslide research is grouped into susceptibility assessment, displacement prediction, and detection. Landslides may be shallow or deep-seated and commonly triggered by rainfall, earthquakes, typhoons, or deforestation [212]. Landslide susceptibility mapping (LSM) uses conditioning factors such as elevation, slope, lithology, soil type, aspect, and distance to roads, faults, and rivers, with steep slopes, weak soils, low shear strength, and river proximity increasing susceptibility [12,213]. Detection maps event location, type, boundary, volume, date, and soil/rock triggers, supporting regional "soft" risk assessment, whereas displacement prediction represents "hard" risk evaluation for specific slopes or assets [214,215]. Traditional detection relied on visual imagery and field surveys [216]. The Frequency Ratio method remains widely used to quantify links between conditioning factors and landslide occurrence, with correlation/multicollinearity checks applied to reduce redundant predictors [217].

AI-driven semi- and fully automated workflows now reduce manual effort and enhance detection and LSM efficiency, especially for pixel-based and object-based image analysis (OBIA) methods [110,213,215]. OBIA generally outperforms pixel-based methods in complex terrain by detecting object-level changes from multi-temporal imagery. For instance, Ghorbanzadeh et al. [110] employed a hybrid ResU-Net–OBIA workflow for landslide detection. In the study, Sentinel-2, NDVI, and slope layers are first segmented using multiresolution segmentation, followed by rule-based OBIA classification to generate object-level candidates. In parallel, ResU-Net performs pixel-wise segmentation to produce probability heatmaps, which are thresholded and fused with OBIA outputs. The hybrid ResU-Net–OBIA approach reduces spectral confusion, enhances boundary delineation, and suppresses false positives compared with standalone ResU-Net or OBIA, demonstrating the value of combining deep semantic segmentation with object-based geomorphological reasoning for landslide mapping.

In other studies, Liu et al. [218] demonstrated that the YOLOv7 model enhanced with a Squeeze-and-Excitation attention mechanism provided higher generalization capability and detected landslides more accurately with fewer missed events. CNNs and RNNs consistently outperform SVM, DT, and RF for LSM [219–221]. Althuwaynee et al. [222] found that a hybrid evidential-AHP (analytical hierarchy process) model outperformed logistic regression. Wang et al. [223] reported that an ensemble of SVM, ANN, and GBoost improved AUC by 0.11–0.35 over single models. Kim and Lee [206] compared CNNs with ML models (RF and bagging) and showed that CNNs consistently achieved higher LSM accuracy. Balogun et al. [102] used meta-heuristic algorithms—GWO, Bat Algorithm (BA), and Cuckoo Optimization Algorithm (COA)—to optimize SVM hyperparameters, improving LSM prediction accuracy. GRU, CNN, and hybrid models (CNN–AEIO [Age of Exploration-Inspired Optimizer], PSO–SVM, SVM–GWO) have also shown strong LSM performance in Lushan, Majiagou, northwest Sichuan, and Jiuxianping [76,106,119,224].

For time-series-based landslide modeling, DNNs, TF-based temporal models, and physics-informed hybrids have improved landslide displacement forecasting; however, models such as GEP, SVM, and RBF often perform poorly when external triggers (e.g., rainfall and reservoir water-level fluctuations) are excluded, limiting their long-term predictive ability [215,225]. GEP has shown superior performance to SVM and RBF in displacement prediction [85]. Comparative DL studies report that transformer models yield the highest accuracy, followed by LSTM, improved Elman networks, RNNs, and other DL architectures [136,158]. The improved Elman network, which incorporates a piecewise time-weighted gradient function, enhances the ability to learn both current and historical temporal dependencies [225].

5.1.3. Sinkholes

Sinkholes are vertical depressions formed by the collapse of overlying soil due to chemical dissolution of underlying karstic bedrock, particularly in carbonate and evaporite terrains [9,214,226]. They display distinct morphologies, such as depth, diameter, circumference, and area, that vary with formation environment and lithology (e.g., basement rock, plateau, and basin sinkholes. Efficient

 doi:10.20944/preprints202605.1511.v1

detection and analysis of sinkhole patterns are essential for disaster mitigation and sustainable development [19,227]. ML/DL applied to subsurface datasets provides a robust means of characterizing sinkhole morphology and distinguishing them from surrounding terrain. Integrated ML/DL models have leveraged diverse data sources, including aerial photographs, GPR, thermal imagery, digital elevation models (DEMs), satellite data, and RGB images [228–231]. In West-Central Florida, Muili and Babaie [232] showed that RF outperformed MLP, SVM, and KNN for sinkhole prediction, and revealed that shallow bedrock depth, land-use patterns, and NW–SE-trending faults were the dominant controls on sinkhole development. Table 6 further provides additional studies on AI applications for sinkhole detection using remote sensing data.

Table 6. Selected studies on AL applications for sinkhole detection using remote sensing data.

Study	Method	Data Utilized	Core Contribution / Key Outcome	Performance	Limitations
[233]	3D CNN	Thermal drone imagery (640×480 px)	Demonstrated the feasibility of using a lightweight 3D CNN model on thermal UAV data to automatically identify artificially created sinkholes	Precision: 87.9%, Recall: 88.1%	Dependent on drone-based thermal surveys; potential omission of sinkholes due to flight speed and background interference; datasets lacked geological variability
[234]	RF	LiDAR (1 m point spacing) and DEM (1.5 m cell size)	One of the earliest works to apply ML to elevation-based sinkhole mapping using LiDAR-derived datasets	Precision: 84.71%, Recall: 65.17%	Poor spatial transferability—accuracy decreased significantly when the model was applied to different regions; high-resolution DEMs are expensive and not easily accessible
[235]	Modified AlexNet CNN	GPR B-scan (50×50 px) and C-scan (50×13 px), enhanced to 200×200 px	Showcased the successful use of CNN for interpreting GPR imagery to detect sinkholes	Precision: 100%, Recall: 100% (with enhanced resolution)	Focused on a localized area; generalization across other locations was not tested; GPR data acquisition is costly and challenging in many karst terrains
[236]	U-Net	LiDAR DEM (1 m)	Developed one of the first U-Net models capable of large-scale sinkhole extraction, mapping >470,000 sinkholes	IoU: 60.4%, Dice: 72.36%	Requires high-resolution LiDAR; ~16% deviation from manual expert mapping; applicability to non-limestone terrains not evaluated

 doi:10.20944/preprints202605.1511.v1

			in Slovenia and later >400,000 in the USA		
[237]	ANN	Optical satellite data + InSAR DEM (10 m)	Applied ANN for both sinkhole detection and susceptibility modeling, highlighting ANN effectiveness for karst hazard assessment	RMSE: 45.1%	DEM accuracy influenced by vegetation and land cover; model performance strongly dependent on DEM quality
[228]	U-Net	LiDAR DEM + aerial imagery (1.524 m/px)	Demonstrated that merging DEM with aerial optical imagery enhances U-Net performance; model transfer successfully applied across different karst regions	IoU: 45.38%, Precision: 66.29%	Limited access to high-resolution LiDAR; performance in non-carbonate terrains remains understudied; imagery alone is insufficient without DEM support

5.2. Case Studies

This section presents real-world cases showing how AI enhances subsurface characterization, hazard prediction, and engineering decisions in EGGE. Each case summarizes: (i) the problem context, (ii) the AI/ML/DL, hybrid, or physics-informed models applied, (iii) multimodal or multisensor data used, and (iv) the value-added gains over conventional methods. These cases reflect the AI–EGGE shift toward data-driven, physics-consistent, and multimodal intelligence for more accurate and decision-ready solutions.

5.2.1. Case 1: Hybrid CNN–ViTF for High-Fidelity, Robust, and Real-Time ERT Inversion

ERT inversion has long been constrained by smoothing artifacts, non-uniqueness, and high computational demand inherent to Gauss–Newton (GN)–based solvers. Yin et al. [41] introduced a Hybrid ViTF–based inversion framework, with spatial CNN blocks and TF self-attention, that transitions ERT imaging from iterative physics-based inversion to a direct, data-driven, image-to-image prediction paradigm with high structural fidelity and real-time performance. The workflow (Figure 13) integrates: (i) large-scale synthetic paired apparent–true resistivity datasets generated through finite-element forward modeling for 1–5 anomalous targets, enabling curriculum training to progressively learn structural complexity; (ii) a residual CNN-based colormap calibration module to predict resistivity ranges for field data where true values are unavailable, ensuring consistent pixel–resistivity mapping; and (iii) the ViTF inversion model that maps calibrated apparent resistivity images to true resistivity distributions (Figure 13a). The detailed ViTF architecture is further illustrated, combining convolutional blocks (Figure 13b) for localized anomaly feature extraction with TF self-attention maps observed apparent-resistivity pseudo-sections to true resistivity distributions for resolving and capturing long-range resistivity dependencies. This architecture overcomes the locality bias and scale sensitivity of CNN-only models and enables generalization across anomaly geometries, contrasts, and spatial configurations. A comparative performance

 doi:10.20944/preprints202605.1511.v1

summary of ViTF against CNN-AE, U-Net, Latent Diffusion Model (LDM), and GN inversion confirmed its superior accuracy, efficiency, boundary preservation, and robustness across all complexity levels.

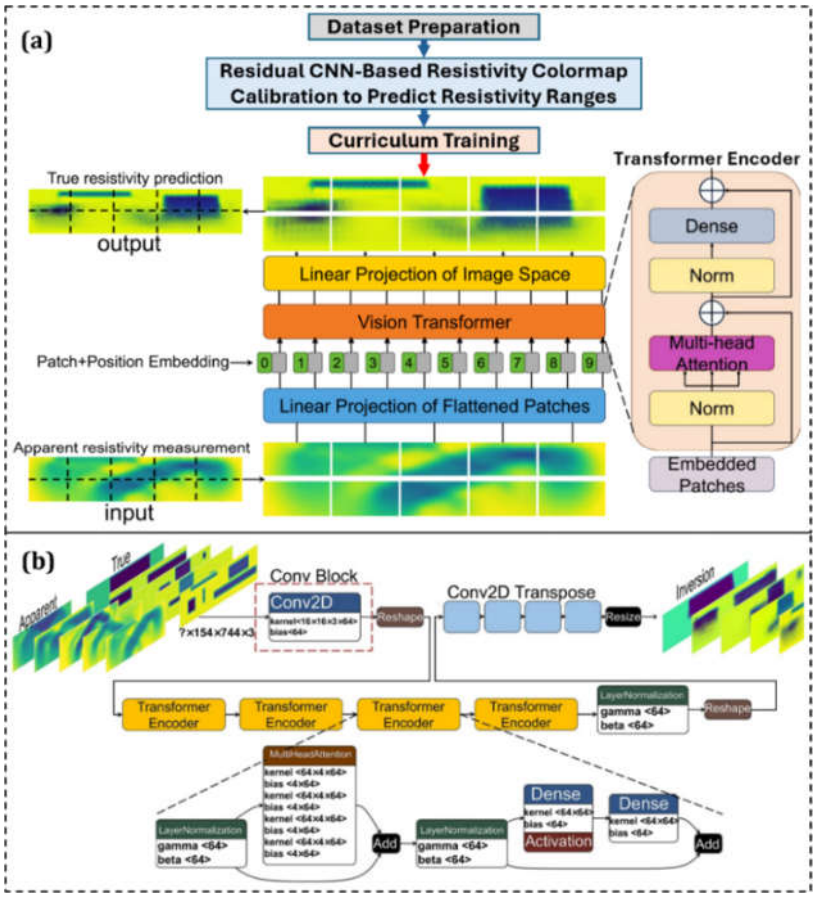

Figure 13. ViTF-based ERT inversion framework with spatial convolutional blocks and TF self-attention for high-fidelity, real-time mapping of apparent resistivity pseudo-sections to true resistivity distributions (modified after [41]). (a) Image-based inversion using calibrated apparent resistivity profiles. (b) CNN–ViTF architecture trained on paired apparent–true resistivity images generated by forward modeling.

The ViTF achieved SSIM up to 0.912, MSE as low as 1.12×10^{-3}, and the shortest training time of 706 s, outperforming CNN-AE and U-Net, which produced blurred anomaly boundaries and higher errors, and outperforming LDM, which showed instability beyond one-target scenarios. It maintained $R^2 > 0.96$ and RMSE < 260 Ωm across 1–5 targets, demonstrating stable high-fidelity inversion with sharp boundary retention. In Figure 14, the colormap calibration module (Panel 1) delivered $R^2 > 0.98$, MAE < 150 Ωm, and RMSE < 260 Ωm, confirming negligible deviation between calibrated and ground-truth colormaps, while inversion results remained statistically unchanged (Panel 2), validating field readiness. Against GN inversion, the ViTF (Panel 3) consistently produced lower pixel-level errors, sharper target geometries, and reduced artifact zones across all five complexity cases, whereas GN exhibited smearing and centroid misplacement of anomalies. Notably, ViTF achieved ~20 ms per inversion, compared to ≥ 5 s per iteration for GN, marking a transition toward real-time ERT imaging. In field validation at the U.S. DOE Hanford Site, ViTF successfully reconstructed key resistivity contrasts associated with stratified vadose-zone heterogeneity and contamination pathways, outperforming GN, which underestimated boundary sharpness and mispositioned anomaly interfaces. While current limitations include reliance on synthetic training data, future integration with PINNs, uncertainty-aware diffusion models, and multimodal joint inversion (e.g., ERT–seismic–GPR) will further enhance generalizability across lithological regimes. This TF-based framework exemplifies the AI-EGGE paradigm shift, where DL models evolve from

 doi:10.20944/preprints202605.1511.v1

post-processing aids to primary inversion engines capable of augmenting or replacing conventional physics-based solvers. The ViTF establishes a new benchmark for rapid, high-resolution, and operationally deployable ERT inversion, enabling real-time decision support for environmental, geotechnical, and subsurface hazard monitoring applications.

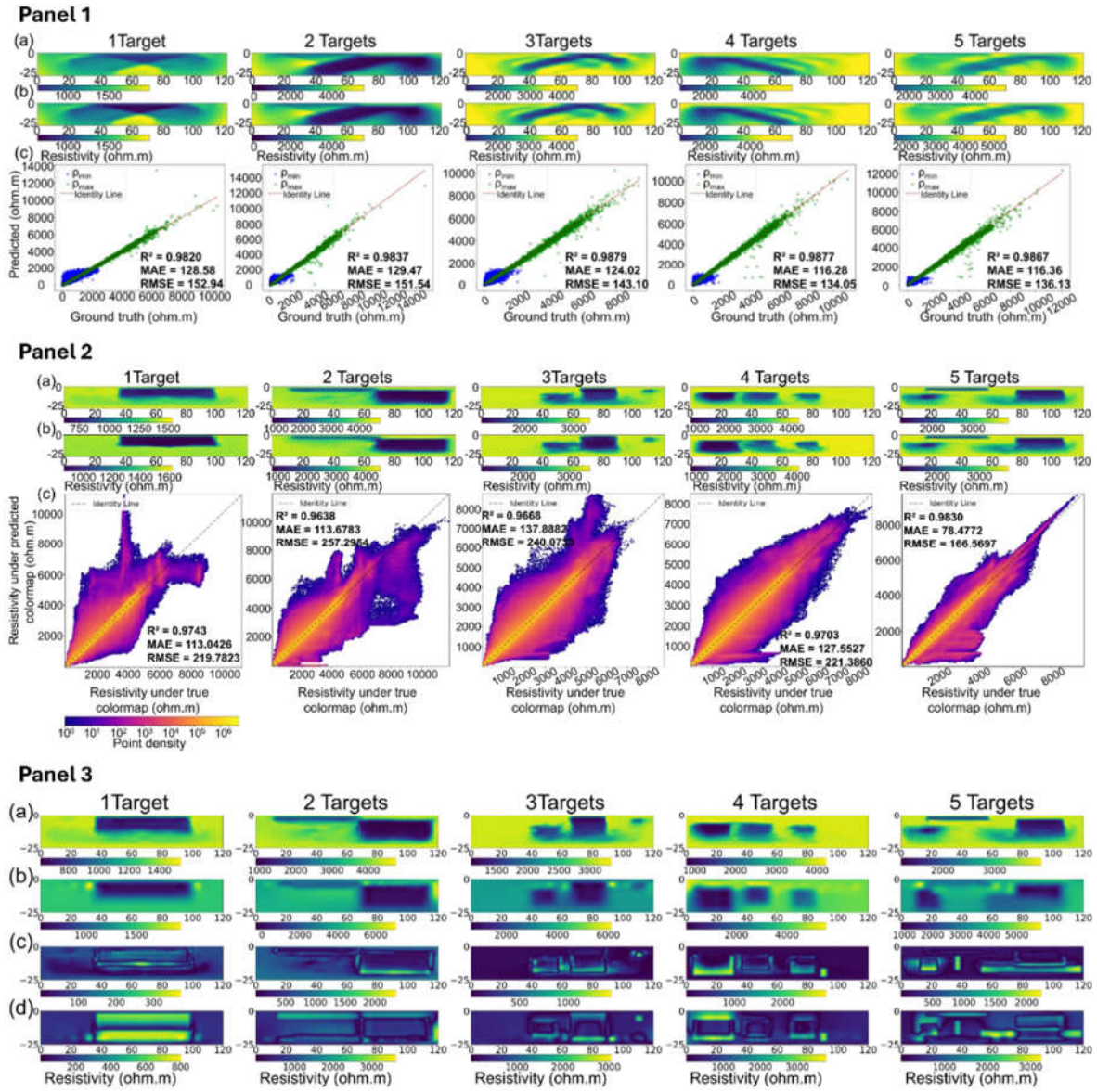

Figure 14. Hybrid ViTF model results and comparison with other DL models (modified after [41]). Panel 1: Predicted upper and lower resistivity colormap limits across the 1–5 target datasets, with green and blue scatters representing the estimated ranges. MAE and RMSE remain generally within 150 Ωm, and R^2 exceeds 0.98 across all complexity levels, indicating minimal calibration error. Sample images show that the predicted colormap (a) produces negligible visual distortion compared with the original apparent resistivity images (b). Panel 2: Scatter-density comparison of pixel-wise inversion resistivity values of ViTF outputs using calibrated versus original colormaps across all target complexities. R^2 values exceed 0.96, with MAE < 140 Ωm and RMSE < 260 Ωm, demonstrating that calibration has no significant impact on inversion accuracy. Panel 3: Example inversion results for 1–5 target datasets obtained using (a) ViTF and (b) GN method, with corresponding error maps for (c) ViTF and (d) GN. ViTF yields sharper anomaly boundaries and lower errors than GN across all complexity levels.

 doi:10.20944/preprints202605.1511.v1

5.2.2. Case 2: Multimodal CNN–TF Fusion for Enhanced Urban Scene and Functional Mapping

Urban scene understanding is critical for land-use mapping, infrastructure planning, and exposure assessment in complex environments; however, remote sensing imagery (RSI) alone often struggles to discriminate morphologically similar urban classes. Su et al. [4] addressed this limitation through a multimodal CNN–Transformer fusion framework that integrates RSI with Points of Interest (POIs) and building footprint data, enabling semantically enriched urban functional mapping. The model employs a dual-branch architecture with attention-weighted fusion and multiscale feature extraction, while a transformer-based interaction module aligns cross-modal representations to enhance feature consistency and contextual awareness.

Experimental results on the Chengdu and Wuhan datasets demonstrate that multimodal integration improves overall accuracy by approximately 6–7% over RSI-only baselines, with consistent gains in Cohen's Kappa, κ, and F1-score. Ablation analysis confirms that attention weighting, modality interaction, and multiscale feature extraction each contribute measurably to performance, while cross-city validation further indicates improved generalization relative to single-modality approaches. Comparative evaluations show that the framework achieves competitive or superior accuracy relative to recent multimodal architectures, with lower model complexity and improved interpretability. Interpretability analysis using Class Activation Maps reveals that multimodal fusion produces more spatially coherent and semantically meaningful attention patterns, particularly for complex functional classes such as commercial, public service, and high-density residential zones, where RSI-only models exhibit ambiguous or diffuse responses. The lightweight design (~6.23M parameters) supports scalable deployment for large-area urban monitoring; however, reliance on static datasets limits temporal adaptability, highlighting the need for integrating dynamic data sources such as mobility patterns and multi-temporal imagery. This case study demonstrates how multimodal fusion within the AI-EGGE paradigm integrates heterogeneous spatial data to improve classification reliability, interpretability, and generalization, strengthening urban analytics for infrastructure exposure assessment and climate–geohazard-informed planning.

6. Challenges and Limitations

Despite major advances, AI–EGGE faces persistent data and fusion-related barriers that limit reliable deployment. Data scarcity, uneven quality, and limited labeled samples—particularly in environmental geophysics, near-surface imaging, and hazard-related applications where ground truth is costly or uncertain—continue to constrain model performance [41,199]. Multimodal fusion must reconcile heterogeneity in spatial support, sampling density, sensor footprint, and noise, especially in shallow, heterogeneous environments, complicating co-registration, scaling, and correlation handling and potentially biasing fused estimates [1,4]. Class imbalance and spatial autocorrelation can inflate apparent accuracy and obscure generalization, while inconsistent metadata, weak documentation, and the lack of standardized multimodal datasets hinder reproducibility, benchmarking, and cross-site transferability [30].

Model robustness, physical consistency, and interpretability remain insufficient for engineering-grade decision-making. Many models trained on site-specific datasets degrade under domain shift, non-stationarity, or extreme triggers, with limited cross-site validation and no widely accepted benchmark datasets for fair comparison [4,100]. Purely data-driven models may violate physical constraints and fail outside the training envelope; although physics-informed, hybrid, and joint inversion approaches improve realism, they remain computationally intensive, often ill-posed, and susceptible to non-unique solutions without informative coupling or priors [115,176]. Modal fusion and deep fusion models raise additional interpretability and black-box concerns for engineering decisions, reinforcing the need for physics-informed and XAI-enhanced mechanisms to produce physically meaningful reasoning for spatiotemporal and multimodal systems—especially for environmental geophysics applications where shallow targets demand high sensitivity to noise,

 doi:10.20944/preprints202605.1511.v1

heterogeneity, and uncertainty [186,192]. UQ is rarely calibrated, limiting confidence and safety-margin assessment for risk-sensitive EGGE applications [165,182].

Operational, regulatory, and institutional barriers continue to slow the translation of AI–EGGE from research to practice. Developing, validating, and maintaining deep or physics-informed models requires specialized expertise, computing resources, and data-annotation capacity that many engineering and environmental agencies lack, while the absence of lightweight, real-time, edge-deployable tools limits early-warning, digital-twin, and on-site applications [17,134,194]. Data sharing restrictions, unclear responsibility for AI-assisted decisions, and limited long-term field pilots further reduce confidence and uptake [186]. In addition, widely relied-upon environmental and engineering standards—such as the European Standards for Structural and Geotechnical Design (Eurocode), the American Association of State Highway and Transportation Officials specifications, the Japanese Geotechnical Society Standards, the Australian Standards for geotechnical and structural design (including AS 1726 and AS 5100), and Environmental Impact Assessment (EIA) regulatory frameworks, currently provide no formal provisions for AI-assisted analyses, constraining regulatory acceptance in design, compliance, and risk management. Similar gaps exist across regional systems, including EIA regimes in Asia, Environmental Management Acts in Africa, and the Environmental Protection and Biodiversity Conservation Act in Australia, which also lack defined pathways for AI-enabled evaluation and decision support. Ethical, cybersecurity, and misuse risks—especially for automated or safety-critical environmental and infrastructure systems—remain unresolved, collectively limiting safe and regulated deployment of AI–EGGE.

7. Future Directions

Advancing AI–EGGE requires moving beyond data-driven prediction toward physics-grounded, uncertainty-aware, real-time, and decision-support AI suitable for field and engineering deployment. Priority lies in maturing physics-integrated learning—through PIML/PINNs, operator-learning networks, and theory-guided hybrids—to reduce non-uniqueness, improve generalization, and stabilize multimodal inversion by embedding governing equations, constitutive relations, and conservation laws directly into learning, even under sparse or noisy data [23,39,171]. Parallel advances in multimodal fusion are expected, with cross-modal attention, foundation-scale multimodal TFs, and GNNs enabling robust integration of geophysical, geotechnical, environmental, and remote-sensing data with differing spatial supports and noise characteristics [4,136,181]. These architectures encode spatial topology, physical neighborhoods, and causal interactions while preserving subsurface structural integrity [108]. When coupled with calibrated uncertainty quantification, interpretability, and physics-based regularization, these architectures can deliver trustworthy models for engineering design, hazard assessment, environmental monitoring, and subsurface digital twins [51,238].

A further frontier is real-time, autonomous, and adaptive geosensing. Edge–cloud computing, IoT-enabled instrumentation, UAV/robotic survey automation, and streaming geophysics will allow continuous assimilation of data for early warning, infrastructure monitoring, and dynamic model updating [53,149,239]. Active learning and adaptive survey designs—guided by model uncertainty—will optimize field campaigns by identifying where to drill, scan, or image to maximize information gain while minimizing cost [1,148]. Progress will also depend on building community-driven multimodal benchmarks, open datasets, and validation protocols tailored to EGGE tasks, along with regulatory and standards development to support safe engineering adoption. Ultimately, the integration of interpretable AI, physics-informed modeling, and real-time digital-twin ecosystems will position AI–EGGE as a core enabler of climate resilience, sustainable urban development, and risk-aware geotechnical and environmental engineering.

Strategic Roadmap for Advancing AI–EGGE:

6. Physics-aligned and trustworthy intelligence: Unify physics-integrated AI (PIML, PINNs, neural operators) with calibrated UQ and interpretable/XAI frameworks to ensure physically consistent, reliable, and audit-ready predictions for engineering-grade deployment.

 doi:10.20944/preprints202605.1511.v1

7. Multimodal fusion and adaptive data ecosystems: Develop next-generation fusion using TFs, GNNs, and cross-modal learning to harmonize geophysical, geotechnical, environmental, and remote-sensing data, supported by adaptive, uncertainty-guided field acquisition that maximizes information efficiency.
8. Autonomous, real-time, and digital-twin EGGE systems: Establish edge–cloud AI platforms, IoT sensing networks, UAV/robotic acquisition, and continuous monitoring to enable real-time hazard detection, early warning, and autonomous digital-twin subsurface systems for resilient infrastructure and environmental management.
9. Standardization, benchmarking, and engineering integration: Create open multimodal benchmarks and validation protocols and co-develop practice-ready AI–EGGE workflows with industry and regulators—embedding safety, due diligence, and codes-of-practice alignment to accelerate formal adoption into engineering standards.

8. Conclusions

AI has catalyzed a decisive shift in EGGE from empirical and deterministic approaches toward data-rich, physics-consistent, and decision-oriented subsurface intelligence. This review synthesizes advances in ML/DL, physics-informed and theory-guided modeling, multimodal data fusion, uncertainty-aware and XAI, and intelligent sensing. Together, these developments enable more accurate and scalable solutions for site characterization, lithological and geotechnical profiling, joint hydrogeomechanical estimation, groundwater and hydro-environmental assessment, geohazard detection, and infrastructure condition monitoring. This trajectory reflects the maturation of AI–EGGE from exploratory algorithms to validated, field-deployable systems supporting early warning, risk-informed design, sustainable infrastructure, and climate-resilient environmental management. The convergence of geophysical, geotechnical, environmental, and data-centric domains now positions AI–EGGE as a core pillar of next-generation subsurface characterization and hazard mitigation.

Responsible, regulated, and engineering-grade deployment, however, remains a critical frontier. Enduring limitations, including data heterogeneity, cross-scale incompatibility, sparse ground truth, lack of standardized multimodal benchmarks, weak generalization across geological and climatic regimes, inadequate interpretability, and limited UQ, continue to constrain confidence, regulatory acceptance, and industry-wide adoption. The absence of formal validation pathways for AI-assisted analyses within environmental and engineering codes and standards underscores the need for auditable modeling frameworks and safety-critical oversight. Future progress must accelerate the integration of physics-based and uncertainty-aware architectures, cross-modal attention and graph-based fusion, digital-twin ecosystems with edge–cloud intelligence, and adaptive sensing strategies that reduce data redundancy while maximizing information value. Realizing the full potential of AI–EGGE requires coordinated efforts across research, practice, regulatory bodies, and international standard-setting organizations to embed rigor, transparency, ethics, and public trust, enabling its transition from a promising innovation to a blueprint for resilient, autonomous, and sustainability-aligned subsurface intelligence.

Acknowledgments: The funding support provided by all contributing agencies that enabled the successful execution of this review is gratefully acknowledged.

Data Availability: All data analyzed during this study are included in this published article.

Ethical Approval: All ethical standards have been duly followed during the research.

Consent to Participate: Not Applicable.

Consent to Publish: Not Applicable.

Financial interests: The authors declare no known competing financial interests or personal relationships that could have appeared to influence the work reported in this paper.

 doi:10.20944/preprints202605.1511.v1

CRediT Author Statement: ASA: Conceptualization, Investigation, Data curation, Resource, Validation, Writing – Original draft, Review & Editing, Funding, & Supervision. **AAB, MDD, BMA, TOA,** & **AOO:** Validation, Resource, Writing – Original draft, Review & Editing.

Notations and Abbreviations

AE	Autoencoder	LIME	Local Interpretable Model-Agnostic Explanations
AI	Artificial Intelligence	LSM	Landslide Susceptibility Mapping
ALE	Accumulated Local Effects	LSTM	Long Short-Term Memory
ANFIS	Adaptive Neuro-Fuzzy Inference System	MASW	Multichannel Analysis of Surface Waves
ANN	Artificial Neural Network	ML	Machine Learning
BNN	Bayesian Neural Network	MLP	Multilayer Perceptron
BPNN	Backpropagation Neural Network	MLR	Multiple Linear Regression
CatBoost	Categorical Boosting	MRF	Multi-Receptive-Field
CNN	Convolutional Neural Network	PIML	Physics-Informed Machine Learning
COA	Cuckoo Optimization Algorithm	PINN	Physics-Informed Neural Network
CPT/CPT-qc	Cone Penetration Test	PISER	Physics-Informed Simple-to-Ensemble Regressor
DAS	Distributed Acoustic Sensing	PNN	Probabilistic Neural Network
DBN	Deep Belief Network	PSO	Particle Swarm Optimization
DFOS	Distributed Fiber-Optic Sensing	RF	Random Forest
DL	Deep Learning	RMQ	Rock Mass Quality
DNN	Deep Neural Network	RNN	Recurrent Neural Network
DRNN	Deep Recurrent Neural Network	RQD	Rock Quality Designation
DT	Decision Trees	SHAP	Shapley Additive Explanations
EBM	Explainable Boosting Machine	SLR	Simple And Multiple Linear Regression
EGGE	Environmental Geophysics and Geotechnical Engineering	SNN	Shallow Neural Network
EM	Electromagnetic Methods	SOM	Self-Organizing Map
ERT	Electrical Resistivity Tomography	SP	Self-Potential
FCN	Fully Convolutional Network	SPT/SPT-N	Standard Penetration Test
FIS	Fuzzy Inference System	SRT	Seismic Refraction Tomography
GA	Generative Algorithm	SVM	Support Vector Machine
GAN	Generative Adversarial Network	TBM	Tunnel Boring Machine
GBM	Gradient Boosting Machine	TDR	Time Domain Reflectometry
GBoost	Gradient Boosting	TEM	Transient Electromagnetic
GEP	Genetic Expression Programming	TF	Transformer
GNN	Graph Neural Network	UAV	Unmanned Aerial Vehicle
GPR	Ground-Penetrating Radar	UQ	Uncertainty Quantification

 doi:10.20944/preprints202605.1511.v1

Grad-CAM	Gradient-Weighted Class Activation Mapping	VAE	Variational Autoencoder
GRU	Gated Recurrent Unit	VGG	Visual Geometry Group Network
GSON	Growing Self-Organizing Network	ViTF	Vision Transformer
GWO	Gray Wolf Optimizer	Vp	P-Wave Velocity
IoT	Internet of Things	Vs	Shear-Wave Velocity
IoU	Intersection over Union	XAI	Explainable AI
IP	Induced Polarization	XGBoost	Xtreme Gradient Boosting
KNN	K-Nearest Neighbors	κ	Cohen's Kappa

References

1. Yu S, Ma J (2021) Deep Learning for Geophysics: Current and Future Trends. Reviews of Geophysics 59:1–36. https://doi.org/10.1029/2021RG000742
2. Kiran Pandiri DN, Murugan R, Goel T (2024) Smart soil image classification system using lightweight convolutional neural network. Expert Systems with Applications 238:122185. https://doi.org/10.1016/j.eswa.2023.122185
3. Sheil B, Anagnostopoulos C, Buckley R, et al. (2026) Artificial intelligence transformations in geotechnics: progress, challenges and future enablers. Computers and Geotechnics 189:107604. https://doi.org/10.1016/j.compgeo.2025.107604
4. Su C, Hu X, Meng Q, et al. (2024) A multimodal fusion framework for urban scene understanding and functional identification using geospatial data. International Journal of Applied Earth Observation and Geoinformation 127:103696. https://doi.org/10.1016/j.jag.2024.103696
5. Meju MA, Gallardo LA (2016) Structural Coupling Approaches in Integrated Geophysical Imaging. In: Integrated Imaging of the Earth: Theory and Applications. Wiley, pp 49–67
6. Balarabe B, Bery AA, Teoh YJ, Khalil AE (2022) New Empirical Approach for the Estimation of Soil Cohesion and Friction Angle in 2D Form for Site Investigations. Sains Malaysiana 51:405–419. https://doi.org/10.17576/jsm-2022-5102-07
7. Kuras O, Wilkinson PB, Meldrum PI, et al. (2016) Geoelectrical monitoring of simulated subsurface leakage to support high-hazard nuclear decommissioning at the Sellafield Site, UK. Science of the Total Environment 566–567:350–359. https://doi.org/10.1016/j.scitotenv.2016.04.212
8. Saadati G, Javankhoshdel S, Mohebbi Najm Abad J, et al. (2024) AI-Powered Geotechnics: Enhancing Rock Mass Classification for Safer Engineering Practices. Rock Mechanics and Rock Engineering. https://doi.org/10.1007/s00603-024-04189-7
9. Bilgilioğlu SS, Gezgin C, Iban MC, et al. (2025) Explainable Sinkhole Susceptibility Mapping Using Machine-Learning-Based SHAP: Quantifying and Comparing the Effects of Contributing Factors in Konya, Türkiye. Applied Sciences 15:3139. https://doi.org/10.3390/app15063139
10. Arif A, Zhang C, Sajib MH, et al. (2025) Rock Slope Stability Prediction: A Review of Machine Learning Techniques. Geotechnical and Geological Engineering 43:124. https://doi.org/10.1007/s10706-025-03091-5
11. Liu C, Macedo J, Rodríguez A (2025) Leveraging physics-informed neural networks in geotechnical earthquake engineering: An assessment on seismic site response analyses. Computers and Geotechnics 182:107137. https://doi.org/10.1016/j.compgeo.2025.107137
12. Shafapourtehrany M, Batur M, Özener H, et al. (2026) Conventional and advanced geospatial techniques for landslide detection and modeling: a comprehensive overview. Geoenvironmental Disasters 13:3. https://doi.org/10.1186/s40677-025-00347-3
13. Akingboye AS, Bery AA, Tang H, et al. (2025) Advancing resistivity–chargeability modeling for complex subsurface characterization using machine learning and deep learning. arXiv (Preprint) arXiv.2509:1–22. https://doi.org/http://doi.org/10.48550/arXiv.2509.17089

 doi:10.20944/preprints202605.1511.v1

14. Dick M, Bery AA, Akingboye AS, et al. (2025) Integrated Machine Learning Modeling of Seismic, Electrical Resistivity, Induced Polarization, and SPT-N Data for Subsurface Integrity Assessment in Granitic Terrain. Earth Systems and Environment. https://doi.org/10.1007/s41748-025-00772-2
15. Ali M, Zhu P, Huolin M, et al. (2024) Data-driven machine learning approaches for precise lithofacies identification in complex geological environments. Geo-spatial Information Science 1–21. https://doi.org/10.1080/10095020.2024.2405635
16. Aydın Y, Işıkdağ Ü, Bekdaş G, et al. (2023) Use of Machine Learning Techniques in Soil Classification. Sustainability 15:2374. https://doi.org/10.3390/su15032374
17. Lu P, Morris M, Brazell S, et al. (2018) Using generative adversarial networks to improve deep-learning fault interpretation networks. The Leading Edge 37:578–583. https://doi.org/10.1190/tle37080578.1
18. Zhao S, Chen Z, Xiong Z, et al. (2025) Beyond Grid Data: Exploring graph neural networks for Earth observation. IEEE Geoscience and Remote Sensing Magazine 13:175–208. https://doi.org/10.1109/MGRS.2024.3493972
19. Alrabayah O, Caus D, Watson RA, et al. (2024) Deep-Learning-Based Automatic Sinkhole Recognition: Application to the Eastern Dead Sea. Remote Sensing 16:. https://doi.org/10.3390/rs16132264
20. Zhang Z, Hu Q, Fang H, et al. (2026) TriGEFNet: A Tri-Stream Multimodal Enhanced Fusion Network for Landslide Segmentation from Remote Sensing Imagery. Remote Sensing 18:186. https://doi.org/10.3390/rs18020186
21. Zhou Z, Gerstoft P, Olsen K (2024) Graph-learning approach to combine multiresolution seismic velocity models. Geophysical Journal International 238:1353–1365. https://doi.org/10.1093/gji/ggae212
22. Ding Y, Chen S, Li X, et al. (2023) Physics-constrained neural networks for half-space seismic wave modeling. Computers & Geosciences 181:105477. https://doi.org/10.1016/j.cageo.2023.105477
23. Chen X-X, Zhang P, Yin Z-Y (2024) Physics-Informed neural network solver for numerical analysis in geoengineering. Georisk: Assessment and Management of Risk for Engineered Systems and Geohazards 18:33–51. https://doi.org/10.1080/17499518.2024.2315301
24. Onyelowe KC, Mojtahedi FF, Ebid AM, et al. (2023) Selected AI optimization techniques and applications in geotechnical engineering. Cogent Engineering 10:. https://doi.org/10.1080/23311916.2022.2153419
25. Khatti J, Grover DKS (2021) Prediction of Geotechnical Properties of Soil using Artificial Intelligence Framework. International Journal of Recent Technology and Engineering (IJRTE) 10:218–227. https://doi.org/10.35940/ijrte.d6625.1110421
26. Linck R, Kale M, Stele A, Schlechtriem J (2025) Testing the Applicability of Drone-Based Ground-Penetrating Radar for Archaeological Prospection. Remote Sensing 17:1498. https://doi.org/10.3390/rs17091498
27. Bala GA, Bery AA, Dick MD, et al. (2025) Modeling subsurface geotechnical integrity via interpolated resistivity–chargeability and SPT datasets with machine learning: A case study from Perak, Malaysia. Physics and Chemistry of the Earth, Parts A/B/C 141:104093. https://doi.org/10.1016/j.pce.2025.104093
28. Hasan M, Su L, Cui P, Shang Y (2025) Development of deep-underground engineering structures via 2D and 3D RQD prediction using non-invasive CSAMT. Scientific Reports 15:1403. https://doi.org/10.1038/s41598-025-85626-7
29. Hoek E, Diederichs MS (2006) Empirical estimation of rock mass modulus. International Journal of Rock Mechanics and Mining Sciences 43:203–215. https://doi.org/10.1016/j.ijrmms.2005.06.005
30. Campos Montero FA, Zuada Coelho B, Smyrniou E, et al. (2025) SchemaGAN: A conditional Generative Adversarial Network for geotechnical subsurface schematisation. Computers and Geotechnics 183:107177. https://doi.org/10.1016/j.compgeo.2025.107177
31. Wu L, Li J, Zhang J, et al. (2024) Prediction model for the compressive strength of rock based on stacking ensemble learning and shapley additive explanations. Bulletin of Engineering Geology and the Environment 83:439. https://doi.org/10.1007/s10064-024-03896-3
32. Shahani NM, Zheng X, Guo X, Wei X (2022) Machine Learning-Based Intelligent Prediction of Elastic Modulus of Rocks at Thar Coalfield. Sustainability 14:3689. https://doi.org/10.3390/su14063689

 doi:10.20944/preprints202605.1511.v1

33. Akingboye AS, Bery AA (2023) Rock mass quality evaluation via statistically optimized geophysical datasets. Bulletin of Engineering Geology and the Environment 82:376. https://doi.org/10.1007/s10064-023-03380-4
34. Akinlalu AA, Futai MM, Afolabi DO, Abraham-A RM (2026) A review on the application of geophysical methods in civil engineering studies. Geosystems and Geoenvironment 5:100453. https://doi.org/10.1016/j.geogeo.2025.100453
35. Giraud J, Lindsay M, Jessell M, Ogarko V (2020) Towards plausible lithological classification from geophysical inversion: Honouring geological principles in subsurface imaging. Solid Earth 11:419–436. https://doi.org/10.5194/se-11-419-2020
36. Akingboye AS (2025) Electrical and seismic refraction methods: Fundamental concepts, current trends, and emerging machine learning prospects. Discover Geoscience 3:87. https://doi.org/10.1007/s44288-025-00169-8
37. Asadi A, Baise LG, Sanon C, et al. (2023) Semi-Supervised Learning Method for the Augmentation of an Incomplete Image-Based Inventory of Earthquake-Induced Soil Liquefaction Surface Effects. Remote Sensing 15:. https://doi.org/10.3390/rs15194883
38. Rasht-Behesht M, Huber C, Shukla K, Karniadakis GE (2022) Physics-Informed Neural Networks (PINNs) for Wave Propagation and Full Waveform Inversions. Journal of Geophysical Research: Solid Earth 127:1–21. https://doi.org/10.1029/2021JB023120
39. Zhou H, Wu H, Sheil B, Wang Z (2025) A self-adaptive physics-informed neural networks method for large strain consolidation analysis. Computers and Geotechnics 181:107131. https://doi.org/10.1016/j.compgeo.2025.107131
40. Zhang R, Zhu W, Li Z, et al. (2024) Re-Net: Multibranch Network With Structural Reparameterization for Landslide Detection in Optical Imagery. IEEE Journal of Selected Topics in Applied Earth Observations and Remote Sensing 17:2828–2837. https://doi.org/10.1109/JSTARS.2023.3344720
41. Yin H, Carroll KC, Yuan Y, et al. (2025) Hybrid Vision Transformer With Convolutional Blocks Approach for Subsurface Electrical Resistivity Tomography Inversion. Journal of Geophysical Research: Machine Learning and Computation 2:1–24. https://doi.org/10.1029/2025JH000734
42. Baghbani A, Choudhury T, Costa S, Reiner J (2022) Application of artificial intelligence in geotechnical engineering: A state-of-the-art review. Earth-Science Reviews 228:103991. https://doi.org/10.1016/j.earscirev.2022.103991
43. Al-Aghbary M, Sobh M, Gerhards C (2022) A geothermal heat flow model of Africa based on random forest regression. Frontiers in Earth Science 10:. https://doi.org/10.3389/feart.2022.981899
44. Ge C, Qin S (2025) Urban flooding digital twin system framework. Systems Science & Control Engineering 13:. https://doi.org/10.1080/21642583.2025.2460432
45. Li Y, Liu X, Zhou J, et al. (2025) Artificial intelligence in traditional Chinese medicine: advances in multi-metabolite multi-target interaction modeling. Frontiers in Pharmacology 16:1–18. https://doi.org/10.3389/fphar.2025.1541509
46. Saneiyan S, Mansourian D (2023) Locating undocumented orphaned oil and gas wells with smartphones. Journal of Applied Geophysics 219:. https://doi.org/10.1016/j.jappgeo.2023.105224
47. Akingboye AS, Bery AA, Kayode JS, et al. (2022) Near-Surface Crustal Architecture and Geohydrodynamics of the Crystalline Basement Terrain of Araromi, Akungba-Akoko, SW Nigeria, Derived from Multi-Geophysical Methods. Natural Resources Research 31:215–236. https://doi.org/https://doi.org/10.1007/s11053-021-10000-z
48. Kemna A, Binley A, Slater L (2004) Crosshole IP imaging for engineering and environmental applications. GEOPHYSICS 69:97–107. https://doi.org/10.1190/1.1649379
49. Chalikakis K, Plagnes V, Guerin R, et al. (2011) Contribution of geophysical methods to karst-system exploration: an overview. Hydrogeology Journal 19:1169–1180. https://doi.org/10.1007/s10040-011-0746-x
50. Müller D, Kwan K, Groves DI (2021) Geophysical implications for the exploration of concealed orogenic gold deposits: A case study in the Sandy Lake and Favourable Lake Archean greenstone belts, Superior Province, Ontario, Canada. Ore Geology Reviews 128:103892. https://doi.org/10.1016/j.oregeorev.2020.103892

 doi:10.20944/preprints202605.1511.v1

51. Davis GB, Rayner JL, Donn MJ (2023) Advancing "Autonomous" sensing and prediction of the subsurface environment: a review and exploration of the challenges for soil and groundwater contamination. Environmental Science and Pollution Research 30:19520–19535. https://doi.org/10.1007/s11356-022-25125-8
52. Sreelakshmi S, Vinod Chandra S ~S. (2026) A hybrid fusion network using convolutional vision transformers for landslide identification. Expert Systems with Applications 298:129688. https://doi.org/10.1016/j.eswa.2025.129688
53. Sharma S, Ahmed S, Naseem M, et al. (2021) A Survey on Applications of Artificial Intelligence for Pre-Parametric Project Cost and Soil Shear-Strength Estimation in Construction and Geotechnical Engineering. Sensors (Basel, Switzerland) 21:463. https://doi.org/10.3390/s21020463
54. Rane N, Choudhary S, Rane J (2023) Leading-edge Artificial Intelligence (AI) and Internet of Things (IoT) technologies for enhanced geotechnical site characterization. SSRN Electronic Journal. https://doi.org/10.2139/ssrn.4640926
55. Jackisch R, Heincke BH, Zimmermann R, et al. (2022) Drone-based magnetic and multispectral surveys to develop a 3D model for mineral exploration at Qullissat, Disko Island, Greenland. Solid Earth 13:793–825. https://doi.org/10.5194/se-13-793-2022
56. Razavi-Termeh SV, Pourzangbar A, Sadeghi-Niaraki A, et al. (2025) Metaheuristic-driven enhancement of categorical boosting algorithm for flood-prone areas mapping. International Journal of Applied Earth Observation and Geoinformation 136:104357. https://doi.org/10.1016/j.jag.2025.104357
57. Gholizadeh A, Saberioon M, Ben-Dor E, Borůvka L (2018) Monitoring of selected soil contaminants using proximal and remote sensing techniques: Background, state-of-the-art and future perspectives. Critical Reviews in Environmental Science and Technology 48:243–278. https://doi.org/10.1080/10643389.2018.1447717
58. Omolaiye GE, Oladapo IM, Ayolabi AE, et al. (2020) Integration of remote sensing, GIS and 2D resistivity methods in groundwater development. Applied Water Science 10:1–24. https://doi.org/10.1007/s13201-020-01219-x
59. Depina I, Jain S, Mar Valsson S, Gotovac H (2022) Application of physics-informed neural networks to inverse problems in unsaturated groundwater flow. Georisk: Assessment and Management of Risk for Engineered Systems and Geohazards 16:21–36. https://doi.org/10.1080/17499518.2021.1971251
60. Phoon K-K (2020) The story of statistics in geotechnical engineering. Georisk: Assessment and Management of Risk for Engineered Systems and Geohazards 14:3–25. https://doi.org/10.1080/17499518.2019.1700423
61. Pradhan B, Lee S (2010) Delineation of landslide hazard areas on Penang Island, Malaysia, by using frequency ratio, logistic regression, and artificial neural network models. Environmental Earth Sciences 60:1037–1054. https://doi.org/10.1007/s12665-009-0245-8
62. Phoon KK, Zhang LM, Cao ZJ (2023) Special issue on "Machine learning and AI in geotechnics." Georisk: Assessment and Management of Risk for Engineered Systems and Geohazards 17:1–6. https://doi.org/10.1080/17499518.2023.2185938
63. Pradhan B, Lee S (2010) Regional landslide susceptibility analysis using back-propagation neural network model at Cameron Highland, Malaysia. Landslides 7:13–30. https://doi.org/10.1007/s10346-009-0183-2
64. Elseicy A, Solla M, Balado J, et al. (2024) Enhancing Reinforced Concrete Bridge Health Monitoring: A Case Study on the Integration of InSAR, GPR, and LiDAR within 3D GIS Environment. ISPRS Annals of the Photogrammetry, Remote Sensing and Spatial Information Sciences X-4/W5-202:155–161. https://doi.org/10.5194/isprs-annals-X-4-W5-2024-155-2024
65. Yin ZY, Jin YF, Shen JS, Hicher PY (2018) Optimization techniques for identifying soil parameters in geotechnical engineering: Comparative study and enhancement. International Journal for Numerical and Analytical Methods in Geomechanics 42:70–94. https://doi.org/10.1002/nag.2714
66. Akingboye AS, Bery AA, Tang H, et al. (2025) Deciphering near-surface architecture and landslide triggers in granitic environments: A regression-driven multiphysics modeling framework for geoengineering integrity. Physics and Chemistry of the Earth, Parts A/B/C 140:104040. https://doi.org/10.1016/j.pce.2025.104040
67. Patel A (2019) Geotechnical Investigations and Improvement of Ground Conditions. Elsevier

 doi:10.20944/preprints202605.1511.v1

68. Habel WR, Krebber K (2011) Fiber-optic sensor applications in civil and geotechnical engineering. Photonic Sensors 1:268–280. https://doi.org/10.1007/s13320-011-0011-x
69. Hong C, Luo G, Chen W (2023) Safety analysis of a deep foundation ditch using deep learning methods. Gondwana Research 123:16–26. https://doi.org/10.1016/j.gr.2022.05.015
70. Lv P, Ma L, Li Q, Du F (2023) ShapeFormer: A Shape-Enhanced Vision Transformer Model for Optical Remote Sensing Image Landslide Detection. IEEE Journal of Selected Topics in Applied Earth Observations and Remote Sensing 16:2681–2689. https://doi.org/10.1109/JSTARS.2023.3253769
71. Chowdhury R, Bhattacharya G, Metya S (2023) Geotechnical Slope Analysis. CRC Press, London
72. Shahin MA (2016) State-of-the-art review of some artificial intelligence applications in pile foundations. Geoscience Frontiers 7:33–44. https://doi.org/10.1016/j.gsf.2014.10.002
73. Shao W, Yue W, Zhang Y, et al. (2023) The Application of Machine Learning Techniques in Geotechnical Engineering: A Review and Comparison. Mathematics 11:1–16. https://doi.org/10.3390/math11183976
74. Akingboye AS, Bery AA, Aminu MB, et al. (2024) Surface–subsurface characterization via interfaced geophysical–geotechnical and optimized regression modeling. Modeling Earth Systems and Environment 10:5121–5143. https://doi.org/10.1007/s40808-024-02054-8
75. Akingboye AS, Bery AA, Tang H, et al. (2025) Machine learning-driven velocity–resistivity modeling: A novel explicit framework for near-surface characterization. Journal of Applied Geophysics 243:105955. https://doi.org/10.1016/j.jappgeo.2025.105955
76. Zhang W, Li H, Tang L, et al. (2022) Displacement prediction of Jiuxianping landslide using gated recurrent unit (GRU) networks. Acta Geotechnica 17:1367–1382. https://doi.org/10.1007/s11440-022-01495-8
77. Jong SC, Ong DEL, Oh E (2021) State-of-the-art review of geotechnical-driven artificial intelligence techniques in underground soil-structure interaction. Tunnelling and Underground Space Technology 113:103946. https://doi.org/10.1016/j.tust.2021.103946
78. Harle SM, Wankhade RL (2025) Machine learning techniques for predictive modelling in geotechnical engineering: a succinct review. Discover Civil Engineering 2:86. https://doi.org/10.1007/s44290-025-00224-w
79. Dikshit A, Pradhan B, Alamri AM (2021) Pathways and challenges of the application of artificial intelligence to geohazards modelling. Gondwana Research 100:290–301. https://doi.org/10.1016/j.gr.2020.08.007
80. Wang N, Zhang H, Dahal A, et al. (2024) On the use of explainable AI for susceptibility modeling: Examining the spatial pattern of SHAP values. Geoscience Frontiers 15:101800. https://doi.org/10.1016/j.gsf.2024.101800
81. Gevaert CM (2022) Explainable AI for earth observation: A review including societal and regulatory perspectives. International Journal of Applied Earth Observation and Geoinformation 112:102869. https://doi.org/10.1016/j.jag.2022.102869
82. Guan Z, Wang Y (2024) Fusion of three-dimensional geotechnical and geophysical data for developing digital twin of underground space. Soils and Foundations 64:101528. https://doi.org/10.1016/j.sandf.2024.101528
83. Searle R, McBratney A, Grundy M, et al. (2021) Digital soil mapping and assessment for Australia and beyond: A propitious future. Geoderma Regional 24
84. Gallardo LA, Meju MA (2003) Characterization of heterogeneous near-surface materials by joint 2D inversion of DC resistivity and seismic data. Geophysical Research Letters 30:. https://doi.org/10.1029/2003GL017370
85. Huang S, Zhou J (2025) Cutting—Edge Soft Computing Technologies for Rock Mass Excavatability: Transforming Prediction with Hybrid GA—MLP and GEP—Based Criteria. Rock Mechanics and Rock Engineering. https://doi.org/10.1007/s00603-025-04760-w
86. Doyoro YG, Gelena SK, Lin C (2025) Improving subsurface structural interpretation in complex geological settings through geophysical imaging and machine learning. Engineering Geology 344:107839. https://doi.org/10.1016/j.enggeo.2024.107839
87. Radwan AE, Wood DA, Radwan AA (2022) Machine learning and data-driven prediction of pore pressure from geophysical logs: A case study for the Mangahewa gas field, New Zealand. Journal of Rock Mechanics and Geotechnical Engineering 14:1799–1809. https://doi.org/10.1016/j.jrmge.2022.01.012

 doi:10.20944/preprints202605.1511.v1

88. Shahin MA (2013) Artificial Intelligence in Geotechnical Engineering: Applications, Modeling Aspects, and Future Directions. In: Metaheuristics in Water, Geotechnical and Transport Engineering, First Edit. Elsevier, pp 169–204
89. Jalal FE, Iqbal M, Khan WA, et al. (2024) ANN-based swarm intelligence for predicting expansive soil swell pressure and compression strength. Scientific Reports 14:14597. https://doi.org/10.1038/s41598-024-65547-7
90. Swetha RK, Bende P, Singh K, et al. (2020) Predicting soil texture from smartphone-captured digital images and an application. Geoderma 376:114562. https://doi.org/10.1016/j.geoderma.2020.114562
91. Penta de Peppo G, Cercato M, De Donno G (2024) Cross-gradient joint inversion and clustering of ERT and SRT data on structured meshes incorporating topography. Geophysical Journal International 239:1155–1169. https://doi.org/10.1093/gji/ggae326
92. Steuer A, Smirnova M, Becken M, et al. (2020) Comparison of novel semi-airborne electromagnetic data with multi-scale geophysical, petrophysical and geological data from Schleiz, Germany. Journal of Applied Geophysics 182:. https://doi.org/10.1016/j.jappgeo.2020.104172
93. Brito da Silva LE, Elnabarawy I, Wunsch DC (2019) A survey of adaptive resonance theory neural network models for engineering applications. Neural Networks 120:167–203. https://doi.org/10.1016/j.neunet.2019.09.012
94. Duan L, Xiong D, Lee J, Guo F (2006) A Local Density Based Spatial Clustering Algorithm with Noise. In: 2006 IEEE International Conference on Systems, Man and Cybernetics. IEEE, pp 4061–4066
95. Shebl A, Abdellatif M, Hissen M, et al. (2021) Lithological mapping enhancement by integrating Sentinel 2 and gamma-ray data utilizing support vector machine: A case study from Egypt. International Journal of Applied Earth Observation and Geoinformation 105:102619. https://doi.org/10.1016/j.jag.2021.102619
96. Delforge D, Watlet A, Kaufmann O, et al. (2021) Time-series clustering approaches for subsurface zonation and hydrofacies detection using a real time-lapse electrical resistivity dataset. Journal of Applied Geophysics 184:. https://doi.org/10.1016/j.jappgeo.2020.104203
97. Charles Komadja G, Westman E, Rana A, Vitalis A (2025) Predicting rock mass strength from drilling data using synergistic unsupervised and supervised machine learning approaches. 18:325. https://doi.org/10.1007/s12145-025-01837-6
98. Warrens MJ, van der Hoef H (2022) Understanding the Adjusted Rand Index and Other Partition Comparison Indices Based on Counting Object Pairs. Journal of Classification 39:487–509. https://doi.org/10.1007/s00357-022-09413-z
99. Zhao Z, Feng W, Xiao J, et al. (2022) Rapid and Accurate Prediction of Soil Texture Using an Image-Based Deep Learning Autoencoder Convolutional Neural Network Random Forest (DLAC-CNN-RF) Algorithm. Agronomy 12:3063. https://doi.org/10.3390/agronomy12123063
100. Yuan B, Choo CS, Yeo LY, et al. (2025) Physics-informed machine learning in geotechnical engineering: a direction paper. Geomechanics and Geoengineering 20:1128–1159. https://doi.org/10.1080/17486025.2025.2502029
101. Schuster GT, Chen Y, Feng S (2024) Review of physics-informed machine-learning inversion of geophysical data. GEOPHYSICS 89:T337–T356. https://doi.org/10.1190/geo2023-0615.1
102. Balogun A-LL, Rezaie F, Pham QB, et al. (2021) Spatial prediction of landslide susceptibility in western Serbia using hybrid support vector regression (SVR) with GWO, BAT and COA algorithms. Geoscience Frontiers 12:101104. https://doi.org/10.1016/j.gsf.2020.10.009
103. Neupane B, Horanont T, Aryal J (2021) Deep Learning-Based Semantic Segmentation of Urban Features in Satellite Images: A Review and Meta-Analysis. Remote Sensing 13:808. https://doi.org/10.3390/rs13040808
104. Yaghoubi E, Yaghoubi E, Khamees A, et al. (2024) A systematic review and meta-analysis of machine learning, deep learning, and ensemble learning approaches in predicting EV charging behavior
105. Sang X, Xue L, Ran X, et al. (2020) Intelligent High-Resolution Geological Mapping Based on SLIC-CNN. ISPRS International Journal of Geo-Information 9:99. https://doi.org/10.3390/ijgi9020099
106. Chou J-S, Nguyen H-M, Phan H-P, Wang K-L (2025) Predicting deep-seated landslide displacement on Taiwan's Lushan through the integration of convolutional neural networks and the Age of Exploration-Inspired Optimizer. Natural Hazards and Earth System Sciences 25:119–146. https://doi.org/10.5194/nhess-25-119-2025

 doi:10.20944/preprints202605.1511.v1

107. Zhong Z, Sun AY, Wu X (2020) Inversion of Time-Lapse Seismic Reservoir Monitoring Data Using CycleGAN: A Deep Learning-Based Approach for Estimating Dynamic Reservoir Property Changes. Journal of Geophysical Research: Solid Earth 125:1–27. https://doi.org/10.1029/2019JB018408
108. Abbaszadeh Shahri A, Chunling S, Larsson S (2024) A hybrid ensemble-based automated deep learning approach to generate 3D geo-models and uncertainty analysis. Engineering with Computers 40:1501–1516. https://doi.org/10.1007/s00366-023-01852-5
109. Jianliang W, Iqbal I, Sanxi P, et al. (2022) Integrated Geophysical Survey in Defining Subsidence Features of Glauber's Salt Mine, Gansu Province in China. Geotechnical and Geological Engineering 40:325–334. https://doi.org/10.1007/s10706-021-01877-x
110. Ghorbanzadeh O, Shahabi H, Crivellari A, et al. (2022) Landslide detection using deep learning and object-based image analysis. Landslides 19:929–939. https://doi.org/10.1007/s10346-021-01843-x
111. Shirmard H, Farahbakhsh E, Heidari E, et al. (2022) A Comparative Study of Convolutional Neural Networks and Conventional Machine Learning Models for Lithological Mapping Using Remote Sensing Data. Remote Sensing 14:819. https://doi.org/10.3390/rs14040819
112. Yao P, Yu Z, Zhang Y, Xu T (2023) Application of machine learning in carbon capture and storage: An in-depth insight from the perspective of geoscience. Fuel 333:126296. https://doi.org/10.1016/j.fuel.2022.126296
113. He Z, Liu H, Wang Y, Hu J (2017) Generative Adversarial Networks-Based Semi-Supervised Learning for Hyperspectral Image Classification. Remote Sensing 9:1042. https://doi.org/10.3390/rs9101042
114. Mojtahedi FF, Yousefpour N, Chow SH, Cassidy M (2025) Deep Learning for Time Series Forecasting: Review and Applications in Geotechnics and Geosciences. Archives of Computational Methods in Engineering 32:3415–3445. https://doi.org/10.1007/s11831-025-10244-5
115. Aleardi M, Vinciguerra A, Hojat A (2021) A convolutional neural network approach to electrical resistivity tomography. Journal of Applied Geophysics 193:104434. https://doi.org/10.1016/j.jappgeo.2021.104434
116. Liu B, Guo Q, Li S, et al. (2020) Deep Learning Inversion of Electrical Resistivity Data. IEEE Transactions on Geoscience and Remote Sensing 58:5715–5728. https://doi.org/10.1109/TGRS.2020.2969040
117. Zhang W, Li H, Li Y, et al. (2021) Application of deep learning algorithms in geotechnical engineering: a short critical review. Artificial Intelligence Review 54:5633–5673. https://doi.org/10.1007/s10462-021-09967-1
118. Iqbal N, Rizwan A, Khan AN, et al. (2021) Boreholes Data Analysis Architecture Based on Clustering and Prediction Models for Enhancing Underground Safety Verification. IEEE Access 9:78428–78451. https://doi.org/10.1109/ACCESS.2021.3083175
119. Zheng H, Liu B, Han S, et al. (2022) Research on landslide hazard spatial prediction models based on deep neural networks: a case study of northwest Sichuan, China. Environmental Earth Sciences 81:258. https://doi.org/10.1007/s12665-022-10369-x
120. Kundu SK, Dey AK, Sapkota SC, et al. (2024) Advanced predictive modelling of electrical resistivity for geotechnical and geo-environmental applications using machine learning techniques. Journal of Applied Geophysics 231:105557. https://doi.org/10.1016/j.jappgeo.2024.105557
121. Fitz S, Romero P (2021) Neural Networks and Deep Learning: A Paradigm Shift in Information Processing, Machine Learning, and Artificial Intelligence. In: The Palgrave Handbook of Technological Finance. Springer International Publishing, Cham, pp 589–654
122. Kurani A, Doshi P, Vakharia A, Shah M (2023) A Comprehensive Comparative Study of Artificial Neural Network (ANN) and Support Vector Machines (SVM) on Stock Forecasting. Annals of Data Science 10:183–208. https://doi.org/10.1007/s40745-021-00344-x
123. Das SK (2013) Artificial Neural Networks in Geotechnical Engineering: Modeling and Application Issues. In: Metaheuristics in Water, Geotechnical and Transport Engineering, First Edit. Elsevier, pp 231–270
124. Kim T, Shin J-Y, Kim H, et al. (2019) The Use of Large-Scale Climate Indices in Monthly Reservoir Inflow Forecasting and Its Application on Time Series and Artificial Intelligence Models. Water 11:374. https://doi.org/10.3390/w11020374
125. Mohebali B, Tahmassebi A, Meyer-Baese A, Gandomi AH (2020) Probabilistic neural networks. In: Handbook of Probabilistic Models. Elsevier, pp 347–367

 doi:10.20944/preprints202605.1511.v1

126. Karpatne A, Ebert-Uphoff I, Ravela S, et al. (2019) Machine Learning for the Geosciences: Challenges and Opportunities. IEEE Transactions on Knowledge and Data Engineering 31:1544–1554. https://doi.org/10.1109/TKDE.2018.2861006
127. Hemdan EE-D, Al-Atroush ME (2024) An efficient IoT-based soil image recognition system using hybrid deep learning for smart geotechnical and geological engineering applications. Multimedia Tools and Applications 83:66591–66612. https://doi.org/10.1007/s11042-024-18230-y
128. Moosavi M, Yazdanpanah MJ, Doostmohammadi R (2006) Modeling the cyclic swelling pressure of mudrock using artificial neural networks. Engineering Geology 87:178–194. https://doi.org/10.1016/j.enggeo.2006.07.001
129. Khanlari GR, Heidari M, Momeni AA, Abdilor Y (2012) Prediction of shear strength parameters of soils using artificial neural networks and multivariate regression methods. Engineering Geology 131–132:11–18. https://doi.org/10.1016/j.enggeo.2011.12.006
130. Attia M, Tsai FTC (2024) Successive bootstrapping deep learning approach and airborne EM-borehole data fusion to understand salt water in the Mississippi River Valley Alluvial Aquifer. Science of the Total Environment 932:172950. https://doi.org/10.1016/j.scitotenv.2024.172950
131. Elakiya N, Keerthana G (2024) Application of Artificial Neural Networks in Soil Science Research. Archives of Current Research International 24:1–15. https://doi.org/10.9734/acri/2024/v24i5674
132. Ge Y, Liu G, Tang H, et al. (2023) Comparative analysis of five convolutional neural networks for landslide susceptibility assessment. Bulletin of Engineering Geology and the Environment 82:377. https://doi.org/10.1007/s10064-023-03408-9
133. Liu M, Liao S, Yang Y, et al. (2021) Tunnel boring machine vibration-based deep learning for the ground identification of working faces. Journal of Rock Mechanics and Geotechnical Engineering 13:1340–1357. https://doi.org/10.1016/j.jrmge.2021.09.004
134. Pi W, Du J, Bi Y, et al. (2021) 3D-CNN based UAV hyperspectral imagery for grassland degradation indicator ground object classification research. Ecological Informatics 62:101278. https://doi.org/10.1016/j.ecoinf.2021.101278
135. Guo QM, Zhan LT, Yin ZY, et al. (2025) Correlation of excavated soil multi-source heterogeneous data using multimodal diffusion model. Acta Geotechnica 20:4977–5005. https://doi.org/10.1007/s11440-025-02690-z
136. Xi N, Yang Q, Sun Y, Mei G (2023) Machine Learning Approaches for Slope Deformation Prediction Based on Monitored Time-Series Displacement Data: A Comparative Investigation. Applied Sciences 13:4677. https://doi.org/10.3390/app13084677
137. Azizi A, Gilandeh YA, Mesri-Gundoshmian T, et al. (2020) Classification of soil aggregates: A novel approach based on deep learning. Soil and Tillage Research 199:104586. https://doi.org/10.1016/j.still.2020.104586
138. Guerri MF, Distante C, Spagnolo P, Taleb-Ahmed A (2025) Boosting hyperspectral image classification with Gate-Shift-Fuse mechanisms in a novel CNN-Transformer approach. Computers and Electronics in Agriculture 237:110489. https://doi.org/10.1016/j.compag.2025.110489
139. Ran X, Xue L, Zhang Y, et al. (2019) Rock classification from field image patches analyzed using a deep convolutional neural network. Mathematics 7:1–16. https://doi.org/10.3390/math7080755
140. Dey B, Ferdous J, Ahmed R (2024) Machine learning based recommendation of agricultural and horticultural crop farming in India under the regime of NPK, soil pH and three climatic variables. Heliyon 10:e25112. https://doi.org/10.1016/j.heliyon.2024.e25112
141. Latifovic R, Pouliot D, Campbell J (2018) Assessment of Convolution Neural Networks for Surficial Geology Mapping in the South Rae Geological Region, Northwest Territories, Canada. Remote Sensing 10:307. https://doi.org/10.3390/rs10020307
142. Lin CS, Chen SH, Chang CM, Shen TW (2019) Crack detection on a retainingwall with an innovative, ensemble learning method in a dynamic imaging system. Sensors (Switzerland) 19:. https://doi.org/10.3390/s19214784
143. Golding VP, Gharineiat Z, Munawar HS, Ullah F (2022) Crack Detection in Concrete Structures Using Deep Learning. Sustainability 14:8117. https://doi.org/10.3390/su14138117

 doi:10.20944/preprints202605.1511.v1

144. Yu Y, Xu T, Shen Z, et al. (2019) Compressive spectral imaging system for soil classification with three-dimensional convolutional neural network. Optics Express 27:23029. https://doi.org/10.1364/OE.27.023029
145. Srivastava P, Shukla A, Bansal A (2021) A comprehensive review on soil classification using deep learning and computer vision techniques. Multimedia Tools and Applications 80:14887–14914. https://doi.org/10.1007/s11042-021-10544-5
146. Tai L, Zhang J, Liu M, et al. (2016) A Survey of Deep Network Solutions for Learning Control in Robotics: From Reinforcement to Imitation. https://doi.org/10.48550/arXiv.1612.07139
147. Tsantekidis A, Passalis N, Tefas A (2022) Front Matter. In: Deep Learning for Robot Perception and Cognition. Elsevier, pp i–iii
148. Liu H, Su H, Sun L, Dias-Da-Costa D (2024) State-of-the-art review on the use of AI-enhanced computational mechanics in geotechnical engineering. Artificial Intelligence Review 57:196. https://doi.org/10.1007/s10462-024-10836-w
149. Mienye ID, Swart TG, Obaido G (2024) Recurrent Neural Networks: A Comprehensive Review of Architectures, Variants, and Applications. Information 15:517. https://doi.org/10.3390/info15090517
150. Wang ZZ, Zhang J, Huang H (2024) Interpreting random fields through the U-Net architecture for failure mechanism and deformation predictions of geosystems. Geoscience Frontiers 15:101720. https://doi.org/10.1016/j.gsf.2023.101720
151. He Y, Semnani SJ (2023) Machine learning based modeling of path-dependent materials for finite element analysis. Computers and Geotechnics 156:105254. https://doi.org/10.1016/j.compgeo.2023.105254
152. Mittal M, Kumar K, Behal S (2023) Deep learning approaches for detecting DDoS attacks: a systematic review. Soft Computing 27:13039–13075. https://doi.org/10.1007/s00500-021-06608-1
153. Santoso B, Anggraeni W, Pariaman H, Purnomo MH (2022) RNN-Autoencoder Approach for Anomaly Detection in Power Plant Predictive Maintenance Systems. International Journal of Intelligent Engineering and Systems 15:363–381. https://doi.org/10.22266/ijies2022.0831.33
154. Yu W, Kim IY, Mechefske C (2021) Analysis of different RNN autoencoder variants for time series classification and machine prognostics. Mechanical Systems and Signal Processing 149:107322. https://doi.org/10.1016/j.ymssp.2020.107322
155. Jozefowicz R, Zaremba W, Sutskever I (2015) An empirical exploration of Recurrent Network architectures. 32nd International Conference on Machine Learning, ICML 2015 3:2332–2340
156. Yang C, Yin Y, Zhang J, et al. (2024) A graph deep learning method for landslide displacement prediction based on global navigation satellite system positioning. Geoscience Frontiers 15:101690. https://doi.org/10.1016/j.gsf.2023.101690
157. Yu Y, Si X, Hu C, Zhang J (2019) A Review of Recurrent Neural Networks: LSTM Cells and Network Architectures. Neural Computation 31:1235–1270. https://doi.org/10.1162/neco_a_01199
158. Niu X, Ma J, Wang Y, et al. (2021) A novel decomposition-ensemble learning model based on ensemble empirical mode decomposition and recurrent neural network for landslide displacement prediction. Applied Sciences (Switzerland) 11:1–18. https://doi.org/10.3390/app11104684
159. Li J, Tang B, Zhang Y, et al. (2025) Study on the influence of lead ions on soil fissure development and intelligent prediction model under dry–wet cycle conditions. Environmental Earth Sciences 84:. https://doi.org/10.1007/s12665-025-12240-1
160. Goodfellow IJ, Pouget-Abadie J, Mirza M, et al. (2014) Generative adversarial nets. Advances in Neural Information Processing Systems 3:2672–2680. https://doi.org/10.1007/978-3-658-40442-0_9
161. Ruan D, Chen X, Gühmann C, Yan J (2023) Improvement of Generative Adversarial Network and Its Application in Bearing Fault Diagnosis: A Review. Lubricants 11:1–21. https://doi.org/10.3390/lubricants11020074
162. Guo S, Wang B, Zhang P, et al. (2023) Influence analysis and relationship evolution between construction parameters and ground settlements induced by shield tunneling under soil-rock mixed-face conditions. Tunnelling and Underground Space Technology 134:105020. https://doi.org/10.1016/j.tust.2023.105020
163. Lyu B, Wang Y, Shi C (2024) Multi-scale generative adversarial networks (GAN) for generation of three-dimensional subsurface geological models from limited boreholes and prior geological knowledge. Computers and Geotechnics 170:106336. https://doi.org/10.1016/j.compgeo.2024.106336

 doi:10.20944/preprints202605.1511.v1

164. Marano GC, Rosso MM, Aloisio A, Cirrincione G (2024) Generative adversarial networks review in earthquake-related engineering fields. Bulletin of Earthquake Engineering 22:3511–3562. https://doi.org/10.1007/s10518-023-01645-7
165. Yan Y, Jiang L, Li J, et al. (2025) Local Information-Driven Hierarchical Fusion of SAR and Visible Images via Refined Modal Salient Features. Remote Sensing 17:2466. https://doi.org/10.3390/rs17142466
166. Biswas A, Md Abdullah Al N, Imran A, et al. (2023) Generative Adversarial Networks for Data Augmentation. In: Data Driven Approaches on Medical Imaging. Springer Nature Switzerland, Cham, pp 159–177
167. Smyrniou E, Coelho BZ (2023) Using Generative Adversarial Networks to create a 2D subsoil schematization. ISMLG
168. Raissi M, Perdikaris P, Karniadakis GE (2019) Physics-informed neural networks: A deep learning framework for solving forward and inverse problems involving nonlinear partial differential equations. Journal of Computational Physics 378:686–707. https://doi.org/10.1016/j.jcp.2018.10.045
169. Karniadakis GE, Kevrekidis IG, Lu L, et al. (2021) Physics-informed machine learning. Nature Reviews Physics 3:422–440. https://doi.org/10.1038/s42254-021-00314-5
170. Zhang H, Song B, Zuo L, Li L (2025) Domain-decomposed physics-informed neural network for one-dimensional soil consolidation under multi-step surcharge loading. Transportation Geotechnics 55:101722. https://doi.org/10.1016/j.trgeo.2025.101722
171. Zhang S, Zhang C, Han X, Wang B (2025) MRF-PINN: a multi-receptive-field convolutional physics-informed neural network for solving partial differential equations. Computational Mechanics 75:1137–1163. https://doi.org/10.1007/s00466-024-02554-5
172. Wang C, Song L han, Yuan Z, Fan J sheng (2023) State-of-the-art AI-based computational analysis in civil engineering. Journal of Industrial Information Integration 33:100470. https://doi.org/10.1016/j.jii.2023.100470
173. Okazaki T, Hirahara K, Ito T, et al. (2025) Physics-Informed Deep Learning for Forward and Inverse Modeling of Inplane Crustal Deformation. Journal of Geophysical Research: Machine Learning and Computation 2:1–13. https://doi.org/10.1029/2024JH000474
174. Lan P, Su J, Ma X, Zhang S (2024) Application of improved physics-informed neural networks for nonlinear consolidation problems with continuous drainage boundary conditions. Acta Geotechnica 19:495–508. https://doi.org/10.1007/s11440-023-01899-0
175. Vahab M, Shahbodagh B, Haghighat E, Khalili N (2023) Application of Physics-Informed Neural Networks for forward and inverse analysis of pile–soil interaction. International Journal of Solids and Structures 277–278:112319. https://doi.org/10.1016/j.ijsolstr.2023.112319
176. Luo K, Zhao J, Wang Y, et al. (2025) Physics-informed neural networks for PDE problems: a comprehensive review. Artificial Intelligence Review 58:323. https://doi.org/10.1007/s10462-025-11322-7
177. Ito S, Fukunaga R, Sako K (2024) Inverse analysis for estimating geotechnical parameters using physics-informed neural networks. Soils and Foundations 64:101533. https://doi.org/10.1016/j.sandf.2024.101533
178. Horiguchi I, Shima K, Okano Y (2025) Physics-informed neural networks (<scp>PINNs</scp>) for high-resolutional prediction of shear stress on cells in suspension culture. AIChE Journal 71:. https://doi.org/10.1002/aic.18853
179. Feng Y, Eun J, Kim S, Kim Y-R (2025) Application of physics-informed neural networks (PINNs) solution to coupled thermal and hydraulic processes in silty sands. International Journal of Geo-Engineering 16:3. https://doi.org/10.1186/s40703-025-00232-w
180. Degen D, Caviedes Voullième D, Buiter S, et al. (2023) Perspectives of physics-based machine learning strategies for geoscientific applications governed by partial differential equations. Geoscientific Model Development 16:7375–7409. https://doi.org/10.5194/gmd-16-7375-2023
181. Liang R, Zhang C, Huang C, et al. (2024) Multimodal data fusion for geo-hazard prediction in underground mining operation. Computers and Industrial Engineering 193:110268. https://doi.org/10.1016/j.cie.2024.110268
182. Castanedo F (2013) A Review of Data Fusion Techniques. The Scientific World Journal 2013:. https://doi.org/10.1155/2013/704504

 doi:10.20944/preprints202605.1511.v1

183. Guo R, Zhou H, Wei X, et al. (2025) Deep joint inversion of multiple geophysical data with U-net reparameterization. GEOPHYSICS 90:WA61–WA75. https://doi.org/10.1190/geo2024-0210.1
184. Jiang Y, Ma J, Ning J, et al. (2025) One-Fit-All Transformer for Multimodal Geophysical Inversion: Method and Application. Journal of Geophysical Research: Machine Learning and Computation 2:. https://doi.org/10.1029/2024JH000432
185. Kuo PC, Chou YT, Li KY, et al. (2024) GNN-LSTM-based fusion model for structural dynamic responses prediction. Engineering Structures 306:117733. https://doi.org/10.1016/j.engstruct.2024.117733
186. Ali S, Abuhmed T, El-Sappagh S, et al. (2023) Explainable Artificial Intelligence (XAI): What we know and what is left to attain Trustworthy Artificial Intelligence. Information Fusion 99:101805. https://doi.org/10.1016/j.inffus.2023.101805
187. Nori H, Caruana R, Bu Z, et al. (2021) Accuracy, Interpretability, and Differential Privacy via Explainable Boosting. Proceedings of Machine Learning Research 139:8227–8237
188. Xiao X, Zou Y, Huang J, et al. (2024) An interpretable model for landslide susceptibility assessment based on Optuna hyperparameter optimization and Random Forest. Geomatics, Natural Hazards and Risk 15:. https://doi.org/10.1080/19475705.2024.2347421
189. Roscher R, Bohn B, Duarte MF, Garcke J (2020) Explainable Machine Learning for Scientific Insights and Discoveries. IEEE Access 8:42200–42216. https://doi.org/10.1109/ACCESS.2020.2976199
190. Dasgupta S, Frost N, Moshkovitz M (2022) Framework for Evaluating Faithfulness of Local Explanations. Proceedings of Machine Learning Research 162:4794–4815
191. Youssef K, Shao K, Moon S, Bouchard L-S (2023) Landslide susceptibility modeling by interpretable neural network. Communications Earth & Environment 4:162. https://doi.org/10.1038/s43247-023-00806-5
192. Agarwal R, Melnick L, Frosst N, et al. (2021) Neural Additive Models: Interpretable Machine Learning with Neural Nets. Advances in Neural Information Processing Systems 6:4699–4711. https://doi.org/https://doi.org/10.48550/arXiv.2004.13912
193. Bortolozo CA, Campaña JDR, Santos FAM Dos, et al. (2024) Joint Inversion of DC and TEM Methods for Geological Imaging. Pure and Applied Geophysics 181:2541–2560. https://doi.org/10.1007/s00024-024-03529-6
194. Lin Y, Yang Q, Li X, et al. (2025) Ice-kNN-South: A Lightweight Machine Learning Model for Antarctic Sea Ice Prediction. Journal of Geophysical Research: Machine Learning and Computation 2:1–17. https://doi.org/10.1029/2024JH000433
195. Attia M, Tsai FTC (2025) Airborne Geophysical and Borehole Data Fusion to Improve Mississippi River Valley Alluvial Aquifer Characterization. Water Resources Research 61:. https://doi.org/10.1029/2025WR040079
196. Lyu B, Wang Y, Miao C, et al. (2025) Fusion of Limited Site-Specific Borehole Logs and Geophysical Data from a Different Site for Three-Dimensional Subsurface Geological Modeling Using Multiscale Generative Adversarial Network. Journal of Geotechnical and Geoenvironmental Engineering 151:. https://doi.org/10.1061/JGGEFK.GTENG-13369
197. Ibraheem IM, Yogeshwar P, Sharifi F, et al. (2025) Joint inversion of transient electromagnetic and radiomagnetotelluric data for enhanced subsurface characterization. Scientific Reports 15:25494. https://doi.org/10.1038/s41598-025-10959-2
198. Ravasi M, Birnie C (2021) A joint inversion-segmentation approach to assisted seismic interpretation. Geophysical Journal International 228:893–912. https://doi.org/10.1093/gji/ggab388
199. Li Y, Xiao X (2025) Deep Learning-Based Fusion of Optical, Radar, and LiDAR Data for Advancing Land Monitoring. Sensors 25:4991. https://doi.org/10.3390/s25164991
200. Kouadio KL, Liu J, Liu R, et al. (2024) K-Means Featurizer: A booster for intricate datasets. Earth Science Informatics. https://doi.org/10.1007/s12145-024-01236-3
201. Lima AAJ, Lopes JC, Lopes RP, et al. (2025) Soil Organic Carbon Assessment Using Remote-Sensing Data and Machine Learning: A Systematic Literature Review. Remote Sensing 17:882. https://doi.org/10.3390/rs17050882

 doi:10.20944/preprints202605.1511.v1

202. Kalantary F, Ardalan H, Nariman-Zadeh N (2009) An investigation on the Su–NSPT correlation using GMDH type neural networks and genetic algorithms. Engineering Geology 104:144–155. https://doi.org/10.1016/j.enggeo.2008.09.006
203. Licznar P, Nearing M. (2003) Artificial neural networks of soil erosion and runoff prediction at the plot scale. CATENA 51:89–114. https://doi.org/10.1016/S0341-8162(02)00147-9
204. Mishra G, Sulieman MM, Kaya F, et al. (2022) Machine learning for cation exchange capacity prediction in different land uses. CATENA 216:106404. https://doi.org/10.1016/j.catena.2022.106404
205. Rastgou M, Bayat H, Mansoorizadeh M, Gregory AS (2022) Estimating Soil Water Retention Curve by Extreme Learning Machine, Radial Basis Function, M5 Tree and Modified Group Method of Data Handling Approaches. Water Resources Research 58:1–26. https://doi.org/10.1029/2021WR031059
206. Kim J-C, Lee S (2023) Comparative Study of Deep Neural Networks for Landslide Susceptibility Assessment: A Case Study of Pyeongchang-gun, South Korea. Sustainability 16:245. https://doi.org/10.3390/su16010245
207. Wang S, Chen Y, Wang M, Li J (2019) Performance Comparison of Machine Learning Algorithms for Estimating the Soil Salinity of Salt-Affected Soil Using Field Spectral Data. Remote Sensing 11:2605. https://doi.org/10.3390/rs11222605
208. Elaziz AEAA, Goda Soliman K, Said Abu-Hashim M, et al. (2023) Enhancing soil salinity prediction in semi-arid regions using machine learning models technology. Ijcbs 24:565–574
209. Zhang Q, Liu M, Zhang Y, et al. (2023) Comparison of Machine Learning Methods for Predicting Soil Total Nitrogen Content Using Landsat-8, Sentinel-1, and Sentinel-2 Images. Remote Sensing 15:2907. https://doi.org/10.3390/rs15112907
210. Lanjewar MG, Gurav OL (2022) Convolutional Neural Networks based classifications of soil images. Multimedia Tools and Applications 81:10313–10336. https://doi.org/10.1007/s11042-022-12200-y
211. Zhang X, Zhu Y, Wang J, et al. (2022) GW-PINN: A deep learning algorithm for solving groundwater flow equations. Advances in Water Resources 165:104243. https://doi.org/10.1016/j.advwatres.2022.104243
212. Liu B, Guo H, Li J, et al. (2024) Application and interpretability of ensemble learning for landslide susceptibility mapping along the Three Gorges Reservoir area, China. Springer Netherlands
213. Das S, Sharma P, Pain A, et al. (2023) Deep learning based landslide detection using open-source resources: Opportunities and challenges. Earth Science Informatics 16:4035–4052.
214. Gutiérrez F, Parise M, De Waele J, Jourde H (2014) A review on natural and human-induced geohazards and impacts in karst. Earth-Science Reviews 138:61–88. https://doi.org/10.1016/j.earscirev.2014.08.002
215. He R, Zhang W, Dou J, et al. (2024) Application of artificial intelligence in three aspects of landslide risk assessment: A comprehensive review. Rock Mechanics Bulletin 3:100144.
216. Carrara A, Cardinali M, Detti R, et al. (1991) GIS techniques and statistical models in evaluating landslide hazard. Earth Surface Processes and Landforms 16:427–445. https://doi.org/10.1002/esp.3290160505
217. Mersha T, Meten M (2020) GIS-based landslide susceptibility mapping and assessment using bivariate statistical methods in Simada area, northwestern Ethiopia. Geoenvironmental Disasters 7:.
218. Liu Q, Wu T ting, Deng Y hong, Liu Z heng (2023) Intelligent identification of landslides in loess areas based on the improved YOLO algorithm: a case study of loess landslides in Baoji City. Journal of Mountain Science 20:3343–3359. https://doi.org/10.1007/s11629-023-8128-0
219. Bui DT, Tsangaratos P, Nguyen VT, et al. (2020) Comparing the prediction performance of a Deep Learning Neural Network model with conventional machine learning models in landslide susceptibility assessment. Catena 188:104426. https://doi.org/10.1016/j.catena.2019.104426
220. Mandal K, Saha S, Mandal S (2021) Applying deep learning and benchmark machine learning algorithms for landslide susceptibility modelling in Rorachu river basin of Sikkim Himalaya, India. Geoscience Frontiers 12:101203. https://doi.org/10.1016/j.gsf.2021.101203
221. Jiang Z, Wang M, Liu K (2023) Comparisons of Convolutional Neural Network and Other Machine Learning Methods in Landslide Susceptibility Assessment: A Case Study in Pingwu. Remote Sensing 15:798.

 doi:10.20944/preprints202605.1511.v1

222. Althuwaynee OF, Pradhan B, Park H-J, Lee JH (2014) A novel ensemble bivariate statistical evidential belief function with knowledge-based analytical hierarchy process and multivariate statistical logistic regression for landslide susceptibility mapping. CATENA 114:21–36. https://doi.org/10.1016/j.catena.2013.10.011
223. Wang Y, Fang Z, Wang M, et al. (2020) Comparative study of landslide susceptibility mapping with different recurrent neural networks. Computers and Geosciences 138:104445. https://doi.org/10.1016/j.cageo.2020.104445
224. Zhang L, Shi B, Zhu H, et al. (2021) PSO-SVM-based deep displacement prediction of Majiagou landslide considering the deformation hysteresis effect. Landslides 18:179–193.
225. Zhang Y, Wang X, Tang H (2019) An improved Elman neural network with piecewise weighted gradient for time series prediction. Neurocomputing 359:199–208. https://doi.org/10.1016/j.neucom.2019.06.001
226. Parise M (2022) Sinkholes, Subsidence and Related Mass Movements, Second Edi. Elsevier
227. Chen H, Oguchi T, Wu P (2018) Morphometric analysis of sinkholes using a semi-automatic approach in Zhijin County, China. Arabian Journal of Geosciences 11:. https://doi.org/10.1007/s12517-018-3764-3
228. Rafique MU, Zhu J, Jacobs N (2022) Automatic Segmentation of Sinkholes Using a Convolutional Neural Network. Earth and Space Science 9:1–15. https://doi.org/10.1029/2021EA002195
229. Jang B, Yoon H-K (2024) Application of infrared thermal images for sinkhole detection with time-series and time-difference index data through a convolution neural network. International Journal of Pavement Engineering 25:. https://doi.org/10.1080/10298436.2024.2317432
230. Kariminejad N, Shahabi H, Ghorbanzadeh O, et al. (2024) Evaluation of Various Deep Learning Algorithms for Landslide and Sinkhole Detection from UAV Imagery in a Semi-arid Environment. Earth Systems and Environment 8:1387–1398. https://doi.org/10.1007/s41748-024-00419-8
231. Jiang Z, Hu S, Deng H, et al. (2024) Detection and automatic identification of loess sinkholes from the perspective of LiDAR point clouds and deep learning algorithm. Geomorphology 465:109404.
232. Muili O, Babaie HA (2025) Sinkhole susceptibility analysis using machine learning for west central Florida. Applied Computing and Geosciences 27:100262. https://doi.org/10.1016/j.acags.2025.100262
233. Lee EJ, Shin SY, Ko BC, Chang C (2016) Early sinkhole detection using a drone-based thermal camera and image processing. Infrared Physics & Technology 78:223–232. https://doi.org/10.1016/j.infrared.2016.08.009
234. Zhu J, Pierskalla WP (2016) Applying a weighted random forests method to extract karst sinkholes from LiDAR data. Journal of Hydrology 533:343–352. https://doi.org/10.1016/j.jhydrol.2015.12.012
235. Kang M-S, Kim N, Im SB, et al. (2019) 3D GPR Image-based UcNet for Enhancing Underground Cavity Detectability. Remote Sensing 11:2545. https://doi.org/10.3390/rs11212545
236. Mihevc A, Mihevc R (2021) Morphological characteristics and distribution of dolines in Slovenia, a study of a lidar-based doline map of Slovenia. Acta Carsologica 50:11–36. https://doi.org/10.3986/ac.v50i1.9462
237. Nefeslioglu HA, Tavus B, Er M, et al. (2021) Integration of an InSAR and ANN for Sinkhole Susceptibility Mapping: A Case Study from Kirikkale-Delice (Turkey). ISPRS International Journal of Geo-Information 10:119.
238. Xixi L, Zou C, Peng C, Wu C (2023) Uncertainty Quantification in Intelligent-Based Electrical Resistivity Tomography Image Reconstruction With Monte Carlo Dropout Strategy. IEEE Transactions on Geoscience and Remote Sensing 61:1–16. https://doi.org/10.1109/TGRS.2023.3262835
239. Ünal İ, Kabaş Ö, Sözer S (2020) Real-time electrical resistivity measurement and mapping platform of the soils with an autonomous robot for precision farming applications. Sensors (Switzerland) 20:251. https://doi.org/10.3390/s20010251